Three instrumental problems in ACAM:

characterisation of the filter set, elimination of scattered light, and design of a new grism.

Annemieke Janssen
Supervisor: Reynier Peletier

23 January 2012

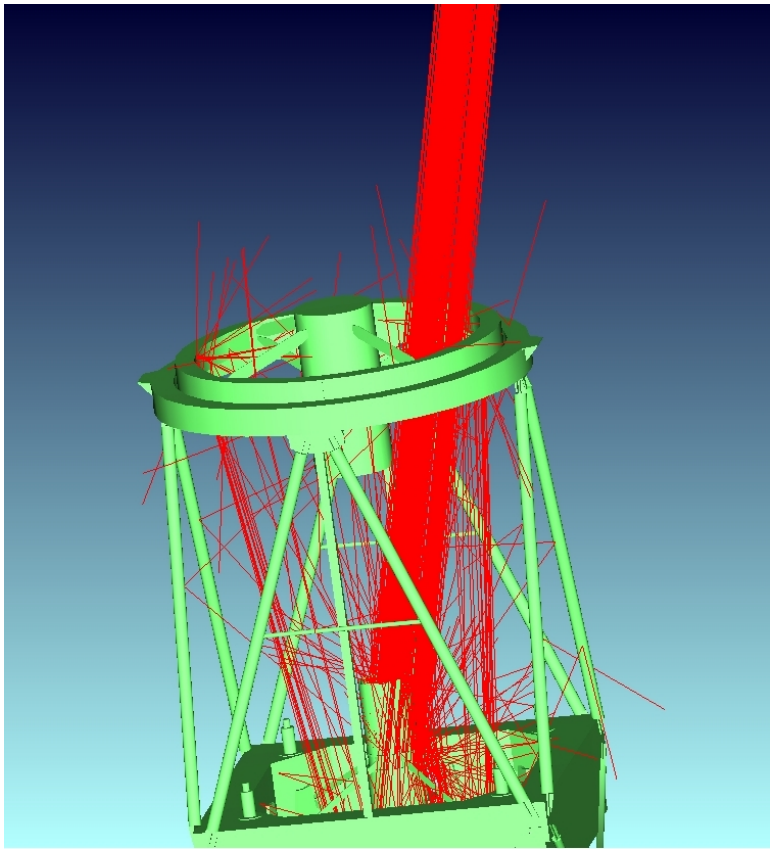

Abstract

ACAM is one of the instruments at the Wiliam Herschel Telescope (WHT) in La Palma. Three problems with this instrument needed investigation and were (partly) solved:

- First the Transmitted Wavefront Distortions (TWDs) of its filters are characterised, because some filters cause bad image quality. The TWD measurements are done with a Shack-Hartmann sensor. Zernike polynomials fitted to the distorted wavefront indicate how apparent the different aberrations are. Some filters contain a high defocus term, but refocussing the telescope with the secondary mirror corrects (at least partly) for the filter defocus. The total of the other 11 measured aberrations is smaller than 0.5λ RMS (Root Mean Square of the TWD) in 84% of the filters, with λ the central wavelength of the filter. An RMS TWD of 0.5λ corresponds to a PSF of 1 pixel on ACAM's ccd for $\lambda = 650$ nm. 0.5λ is therefore taken as the dividing line between bad and good filters.
- Second the scattered light in ACAM, which is clearly apparent in imaging mode, is investigated. It is caused by reflections of moonlight on the inside of the telescope baffles, and light-trap baffles are required to eliminate it. After testing some cardboard baffles it was decided to make a light-trap baffle in the tube under the Nasmyth fold mirror. The baffle reduces the scattered light intensity by 70% at the cost of 10% vignetting of the autoguider. This is some improvement, but not sufficient so further investigations continue.
- Finally two prisms, which will be placed next to a Volume Phase Holographic (VPH), are designed. The material and angles should be chosen such that the throughput and resolution in the blue are better than the current VPH assembly. Simulations in Zemax resulted in the final design: 2 prisms made of BK7 with a prism angle of 13.708 degree. The VPH assembly, also called grism, is placed in ACAM and tested.

This report has been written as part of the master Astronomy at the Rijksuniversiteit Groningen, The Netherlands.

Contents

1 Introduction

On top of a mountain in La Palma, we find an observatory with telescopes from countries all over the world. The Isaac Newton Group of telescopes (ING) owns three of them: the Isaac Newton Telescope (INT), the William Herschel Telescope (WHT), and the Jacobus Kapteyn Telescope (JKT). Of these three the WHT is the largest with a 4.2 metre diameter primary mirror, and it is used extensively for different kinds of optical and infrared observations. In addition to being the largest, it is also the youngest telescope of the three. Construction began in the UK in 1983, and it saw its first light in La Palma in 1987. The WHT has different instruments that can be mounted to it: imagers, spectrographs, a multi-object fibre spectrograph, and an adaptive optics system.

All these instruments are placed at one of the three foci of the WHT: prime focus, Cassegrain focus, or Nasmyth focus. The primary mirror focuses science light on prime focus. Besides an instrument, also the secondary mirror can be placed here. This turns the telescope into Cassegrain mode. The secondary directs the light through a hole in the primary mirror to the instruments that are mounted below the primary (this is illustrated in Section 2). The last possibility is Nasmyth focus, in which case light is also focused by the primary and the secondary mirror. It is different from Cassegrain focus because now a flat mirror, placed above the primary, intercepts the light and directs it to the sides. There the light is focused in one of the two Nasmyth focal stations. These rooms include the larger instrumentation like the adaptive optics system.

We leave the prime and Nasmyth focus for what they are for this moment, and concentrate on Cassegrain focus. After passing the primary mirror, the light reaches the Acquisition & Guiding box (or shortly A&G box). This box contains a flat mirror for directing light to ACAM, a folded Cassegrain instrument. The flat mirror is on purpose too small to intercept all the light. As a result, part of the light continues to the autoguider which observes from 7.3 to 12.1 arc minutes from telescope pointing. Some instruments (ISIS, LIRIS and any visiting instruments) are located right under the A&G box and do not need the flat mirror. The A&G box will be discussed in more detail in Section 2.

One of the instruments at Cassegrain focus is ACAM which was only commissioned a few years ago, in June 2009. ACAM is an imager as well as a low resolution spectrograph. One can easily switch it from imaging to spectroscopy by placing a grism in the science beam. A grism consists of a Volume Phase Holographic (VPH) with a prism on either side of it. A VPH works similar to a transmission grating, section 5 will treat the working of

VPHs in more detail. High dispersion VPHs can be produced, resulting in a compact and powerful grism. One grism is permanently placed in one of the ACAM filter wheels, making switching between imaging and spectroscopic mode a matter of seconds.

There were three issues with ACAM which needed some investigation. These are:

1. Some filters produce low quality images when ACAM is in imaging mode. Stars are blurred instead of being sharp points. This is possibly because of wavefront aberrations introduced by the filters. Filters are not the only objects introducing aberrations: it happens in the atmosphere and the telescope as well. Until the science light reaches the earth's atmosphere it can be considered a series of flat wavefronts. These are slightly distorted by turbulence in the air. Also the telescope and instrument optics introduce wavefront aberrations. During the design process these aberrations are reduced so that they do not significantly degrade the image quality at best seeing.

   The filters that are used in ACAM have not been chosen specifically to keep aberrations small, so it would be a good start to measure the aberrations in the filters first. If the results indeed match the observations, we decide upon the maximum acceptable error (The Transmitted Wavefront Error as discussed in Section 3) and only use the good filters. Some aberrations can perhaps be corrected for; it might be possible to refocus with the secondary mirror if a filter contains a defocus term. Finally the measurement data and our conclusions will be made public in the filter database of the ING, so that observers can use it when preparing their observations.

2. The next issue is moonlight leaking into ACAM. If the moon is between 4 and 30 degrees away from telescope pointing, observations contain arcs and spots in the images. With a full moon at zenith this is obviously a problem for many observations. The problem has been there since ACAM's first light, and it is not or less apparent in other instruments. Does this mean that there is a light leak in ACAM itself? Or is it just better visible than in other instruments because of some characteristics of ACAM? Stray light is a common problem in telescopes, which is why many contain baffles to stop stray light reaching the instruments. This might be necessary in the WHT as well, in which case we need to know which parts of the telescope or which instruments can be baffled. Section 4 describes the tests that were performed in order to find this.

3. The final issue was not as much as a problem but more of a modification in ACAM. The spectrograph had a resolution of 450 for an 1

arcsecond slit and a wavelength of 600 nm. As said before, the dispersing element is a grism consisting of a VPH and two prisms. With another VPH the resolution could be higher, and the efficiency in the blue could be better. There were already plans for this new grism and a VPH had been bought. The next steps include the design of the two new prisms, ordering them, and aligning the completed grism in ACAM.

These issues are described in the subsequent sections, after an introduction to the telescope and instrument.

2 Telescope and instrument design

There are three issues in ACAM to be addressed: The characterisation of the wavefront aberrations introduced by the filters, the scattered light when the moon is close to telescope pointing, and the design of a second grism. For all these issues it is important to know how the WHT and ACAM work, and how they are connected. Therefore this section gives a detailed description of the telescope and instrument.

2.1 William Herschel Telescope

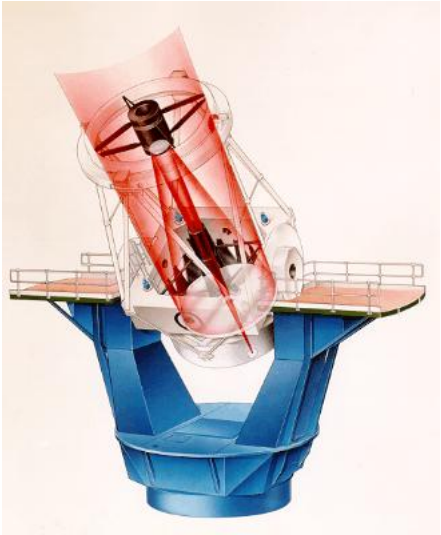

Figure 1: The light path of a distant object to Cassegrain focus. *Image courtesy of the Isaac Newton Group of Telescopes, La Palma.*

Figure 1 shows the light path when one observes at Cassegrain focus. The light of a distant object first hits the 4.2 metre paraboloid primary mirror which is supported by the primary mirror cell. The primary reflects the light to the secondary, from where it is directed back through a hole in the primary mirror. The secondary mirror can be replaced by a prime focus instrument, but this rarely happens; the WHT is mostly used in Cassegrain or Nasmyth mode. The secondary mirror is not completely fixed, it can move with steps of 0.02 mm for focusing the light beam on any of the Cassegrain/Nasmyth instruments. A baffle around the secondary mirror, in the shape of a short cylinder, prevents stray light from reaching the mirror. Often the length of such a baffle is a trade-off; the longer it is, the less stray light reaches the mirror. But it will also block out science light coming from the primary mirror, directed at an edge of the secondary mirror. Baffling the telescope efficiently without losing science light is therefore quite a challenge.

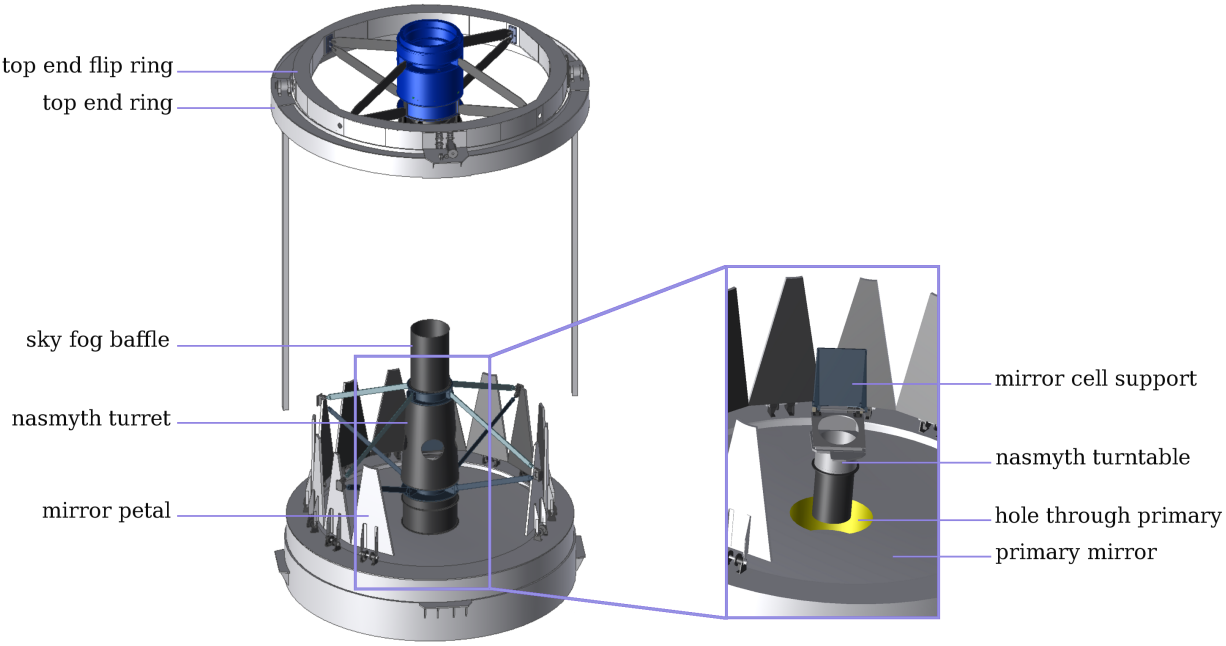

Figure 2: The telescope as seen from above. The Nasmyth turret and sky fog baffle are invisible in the enlarged area to show the hidden optics: the Nasmyth turntable and the Nasmyth mirror support. In this image the Nasmyth mirror does not intercept the light beam so the telescope is in Cassegrain mode. *Edited with a student version of Autodesk Inventor.*

Before the science light reaches the hole in the primary mirror it first passes the sky fog baffle (see figure 2). The sky fog baffle is an extension of the Nasmyth turret which prevents non-science light from reaching the optics in the Nasmyth turret and in the Acquisition&Guiding (A&G) box. Non-science light can originate from a bright source in the sky like the moon or a planet, or it can be reflected by bright parts like the dome, trusses, or mirror edges. Again the length of the baffle is a trade-off; a longer baffle rejects more non-science light, but too long a baffle blocks out science light from the primary to the secondary mirror. In fact this happens already: the sky fog baffle vignettes a bit. The Nasmyth turret contains a small flat mirror on a turntable which can direct the light through one of the three holes in the turret. Two sides are used for instruments at the Nasmyth foci, one is for a free port. The Nasmyth focal stations are mainly used for large instruments and the adaptive optics system. These instruments are not attached to the telescope directly, but are placed in a station on the telescope mount. An image derotator or turntable, when placed in the light beam, corrects for field rotation.

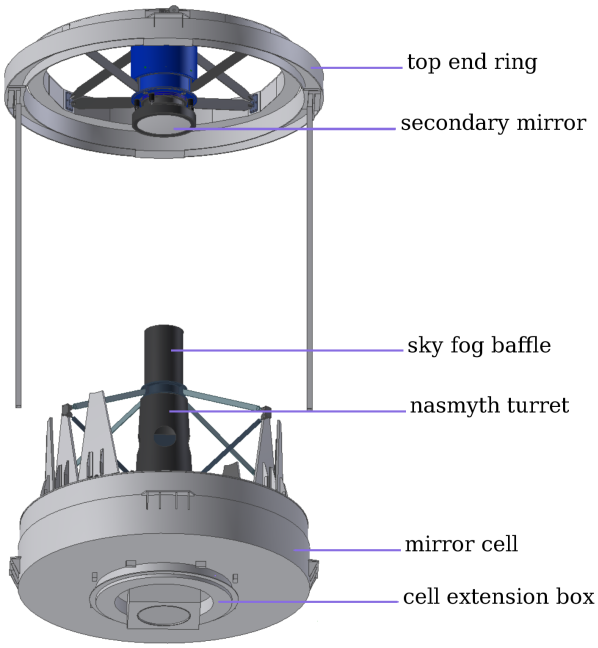

Figure 3: The telescope as seen from below. *Edited with a student version of Autodesk Inventor.*

One easily turns the telescope from Nasmyth mode into Cassegrain mode by folding the flat mirror in the Nasmyth turret away. Light then passes through the primary mirror and the mirror cell. Below the mirror cell sits the extension box. The box contains a turntable, and connects to the A&G box. Figure 3 shows some of these components.

2.2 Acquisition & Guiding box

ACAM and other Cassegrain instruments, like ISIS and LIRIS, are mounted to the A&G box. ISIS and LIRIS are attached directly under the A&G box, so the light goes straight through the box to the instruments. ACAM, on the other hand, is mounted at one of the three free ports on the side. An elliptical fold mirror in the box directs the science light into ACAM. Moreover the box contains a camera to view the ISIS slit, comparison lamps, and an autoguider. Figure 4 shows the contents of the A&G box. The elliptical mirror in the centre of the A&G box is not fixed; it is mounted on a turntable so it can direct the light to any of the three free ports. Moreover it can move out of the way for the smaller mirror (ACam Cal, small feed) which is used for the calibration lamps. As mentioned in the Introduction, the mirror used during observations is too small to intercept the whole Field of View. The FoV of the mirror is only 10.3 arcminutes while an unvignetted FoV of 18.1

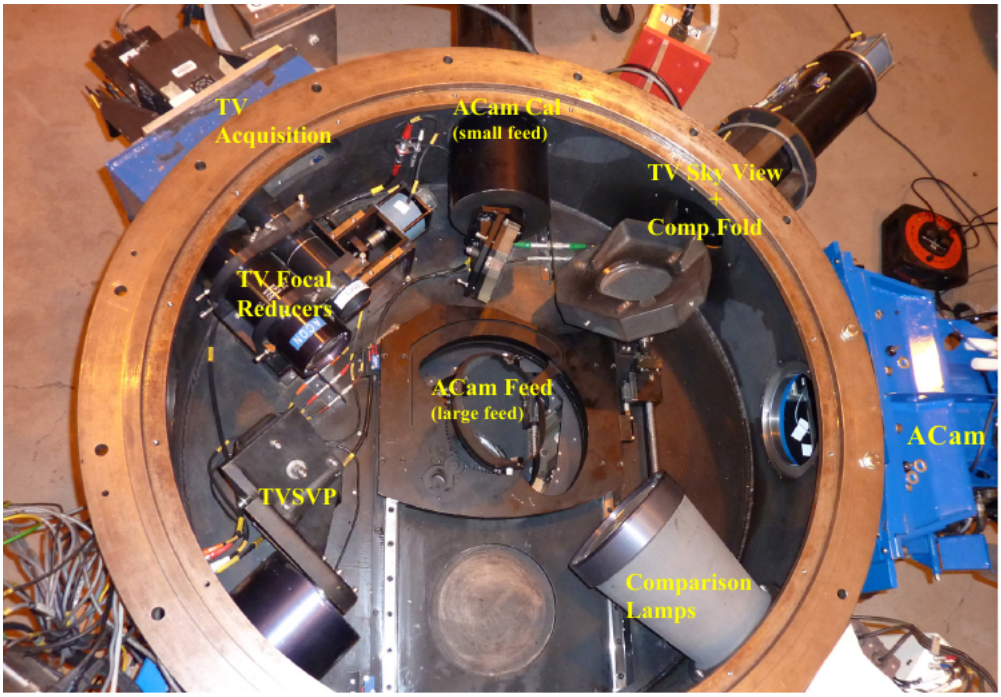

Figure 4: The A&G box seen from above, as it will be attached to the telescope. The light hits the flat mirror in the middle (called ACAM Feed) and is directed to ACAM on the right.

arcminutes is available. All light passing the 10.3 arcminutes mirror goes to the autoguider. The centre of the autoguider field moves between 8.2 and 11.2 arcminutes from telescope pointing. With a field diameter of 1.8 arcminutes, it follows that the autoguider reaches from 7.3 to 12.1 arcminutes radius, or 14.6 to 24.2 arcminutes FoV. Clearly the autoguider is vignetted at the edges, but this is only by 5% as one can see in the vignetting plot in figure 5. The figure was made with Zemax, an optical design programme. A short description of Zemax is given below.

Zemax is an optical design programme which predicts the performance of optical systems, like telescopes and instruments, with the use of ray tracing. It draws all optical components of the system, and traces rays from one to the next surface till they reach the detector. Usually this is done in sequential mode, meaning that the user defines from which to which surface the rays are traced. Any ray that is blocked or falls out of reach of the next optical surface, will stop being traced. One can thus investigate the vignetting of the telescope for all FoVs of interest, and visualise it in a vignetting plot like the one in figure 5. It shows not only when vignetting occurs, but also how bad it is, taking into account the size of the mirrors, the baffles, and the transmission in glass.

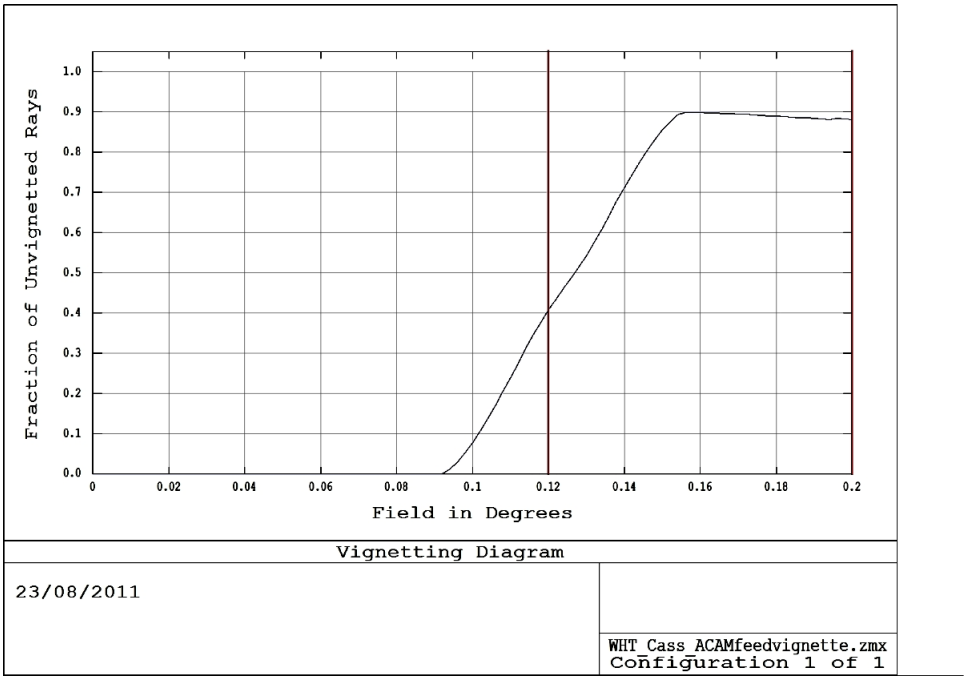

Figure 5: Vignetting plot for the autoguider. Note that the radius is given in degrees on the x-axis, and that the edges of the autoguider FoV are marked with vertical lines. Vignetting is caused by the ACAM feed mirror at small radii, and by the sky fog baffle at large radii.

If we are only interested in the unvignetted FoV, Zemax is not necessary because the FoV can easily be calculated by hand. All Field of Views mentioned above have been calculated this way from geometry, and rounded off to one tenth of an arc minute. In order to do so, one first needs to know the plate scale (PS) on the detector in arcseconds/mm. This number translates the physical area on the ccd in mm to the observed field on the sky in arcseconds, and it is given by[8]:

$$PS = \frac{206265}{f} \text{ arcsec/mm} \tag{1}$$

with f the effective focal distance in mm. In the WHT $f = 45738$ in Cassegrain focus, resulting in a PS of 4.51 arcsec/mm. The effect of an aperture between the secondary mirror and the ccd is showed in figure 6. D is the diameter of the secondary mirror, which is 1001 mm. The distance from the secondary mirror to focus is 10535 mm, d is the diameter of the aperture, and x is the separation between the aperture and focus. The sky fog baffle restricts the FoV most, having a diameter of 710 mm, located at 6500 mm from focus. With an unvignetted diameter at the detector of 241 mm this implies a FoV of 1088 arc second or 18.1 arcminutes. This does

not mean that larger angles cannot be observed, only that the intensity at these angles drops. The exact amount of vignetting, including effects of the baffles and throughput of optical elements, can only be found with Zemax.

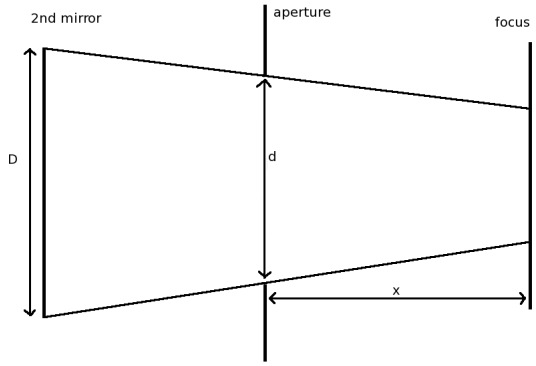

Figure 6: Unvignetted FoV of an aperture placed between the secondary mirror and the focal plane.

2.3 ACAM

ACAM is an 8.3 arcminutes FoV imager and spectrograph which was commissioned in June 2009. It replaced the former auxiliary-port imager which had a 1.8 arcminutes FoV only. Since a larger FoV is available at Cassegrain focus, ACAM was designed to benefit better from this. Besides having a larger field of view, ACAM contains more filters and it is easier to change them. The old camera had only place for six 50 mm filters, while in ACAM eleven filters with sizes of 50 mm, 76 mm, and 63 mm can be used. Moreover ACAM contains permanently a Volume Phase Holographic (VPH) in one of the filter wheels to provide low resolution spectra (Resolution = 290 and 570 for λ = 380 and 750 mm respectively). This possibility to change quickly from an imager to a spectrograph makes the instrument very flexible. ACAM is mounted permanently at folded Cassegrain focus so it can be used any time the telescope is in Cassegrain mode. Since this is the case most of the time, ACAM is suitable for override programmes and programmes requiring rapid response. All this flexibility is a result of the design which had to fit a broad range of science cases.

Figure 7 shows a transparent view of ACAM. Light enters the instrument from the left, through the first focal plane. A slit or clear aperture is placed in the focal plane, and after that there is a filter holder which can contain two filters (see figure 8 for the slits and clear apertures in ACAM's focal plane). The filter holder can contain 2 filters only because this is not the common place for normal filters. Only narrow-band interference filters are

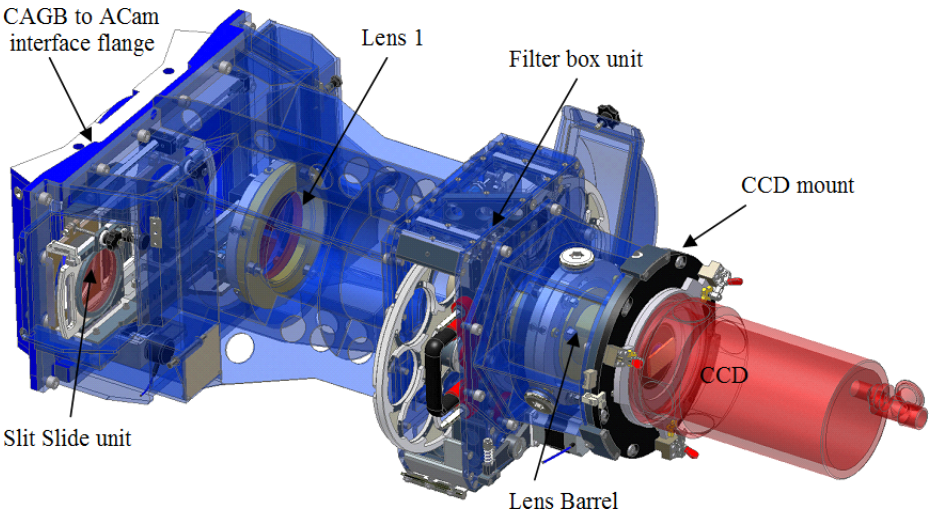

Figure 7: Overview of ACAM; light goes from the left to the right. Two narrow band filters can be placed in the slit slide unit. Its total length is 1.2 metres.

placed here because they suffer from vignetting when placed in a filter wheel. Most filters that fit in ACAM are broad band filters; a piece of coloured glass with an anti-reflection coating on it. Narrow band filters work differently because the throughput curve needs to peak at a specific wavelength and to have a small FWHM. Especially the H-alpha filters and Taurus filters, which range from 373 nm till 689 nm, can have a FWHM as small as a few nanometres. In order to see why these filters suffer from vignetting when placed in the filter wheel, we need to know how interference filters work.

The principle of interference filters is illustrated in figure 9. Light arrives under an angle of incidence i, and is transmitted in a medium with index n_1 at an angle t. The optical path length difference between T_0 and T_1 is [5]:

$$\Delta\Lambda = \frac{2n_1 d}{\cos(t)} - n_0(\overline{AC}) \text{ with } (\overline{AC}) \text{ the distance between A and C.}$$

Find an expression for $(\overline{AC})$ first:

$$(\overline{AC}) = (\overline{AB})\sin(i) = (\overline{AB})\frac{n_1}{n_0}\sin(t)$$

And with $(\overline{AB}) = 2d \cdot \tan(t) = 2d \cdot \frac{\sin(t)}{\cos(t)}$ we get:

$$(\overline{AC}) = \frac{2dn_1}{n_0}\frac{\sin^2(t)}{\cos(t)}$$

The difference in optical path length is thus:

$$\Delta\Lambda = \frac{2dn_1}{\cos(t)} \cdot (1 - \sin^2(t)) = 2dn_1\cos(t) \qquad (2)$$

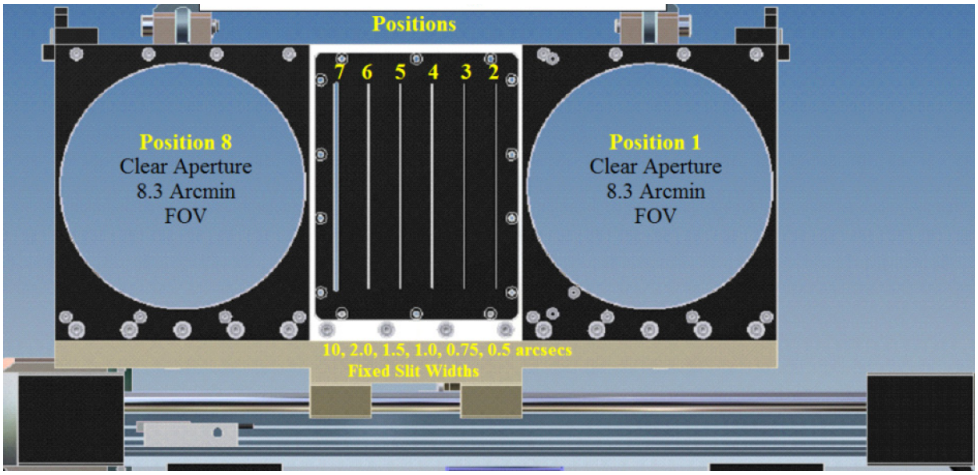

Figure 8: Slit view at the entrance of ACAM, showing the slit mask with six different slits (with sizes 0.5, 0.75, 1.0, 1.5 , 2, 10 arc seconds) and the clear apertures.

Constructive interference occurs for wavelengths λ with $\Delta\Lambda = m \cdot \lambda$, m being an integer. These wavelengths are transmitted completely, while other wavelengths are transmitted partly or cancel each other out. Only one layer does not produce a narrow band filter with only a few nm FWHM, so multiple layers are stacked to restrict the transmitted wavelength. The index of refraction and thickness of the layers determine the transmittance curve with a specific central wavelength and FWHM. These properties hold for normal incidence ($i = 0$) only; for any non-zero angle of incidence, the transmitted wavelength shifts to the blue. This is immediately clear from the just derived equation $\lambda_i = 2dn_1 \cos(t)$. Usually the blue-shift is given as function of incidence angle instead of transmitted angle:

$$\lambda_i = 2dn_1 \cos(t)$$

Using Snell's law, $n_0 \sin(i) = n_1 \sin(t)$, this becomes:

$$\begin{aligned}
\lambda_i &= 2dn_1 \cos(\sin^{-1}(\frac{n_0 \sin(i)}{n_1})) \\
&= 2dn_1 \sqrt{\cos^2(\sin^{-1}(\frac{n_0 \sin(i)}{n_1})} \\
&= 2dn_1 \sqrt{1 - \sin^2(\sin^{-1}(\frac{n_0 \sin(i)}{n_1}))} \\
&= 2dn_1 \sqrt{1 - (\frac{n_0}{n_1})^2 \sin^2(i)}
\end{aligned}$$

So:

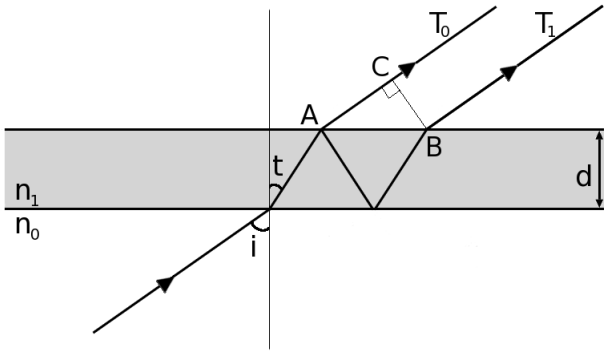

Figure 9: Interference filter with index n_1, angle of incidence i, and thickness d.

$$\lambda_i = \lambda_0 \sqrt{1 - (\frac{n_0}{n_1})^2 \sin^2(i)} \tag{3}$$

A non-zero incidence angle causes a blue-shift in the transmitted wavelength of the filter. This is a problem in the pupil plane, where the filter wheels are located. An on-axis source beam arrives under normal incidence at the filter, but an off-axis source beam doesn't (see figure 10 for the light paths of an on-axis and off-axis source beam). The blue-shift at the edge of the FoV is only a few nanometres (2 nm for 4 arc minute when $n = 1.5$), but this can be more than the FWHM of the filter. As a result, the observed wavelength is invisible at the edges of the FoV. The best solution is to place these narrow-band filters in the focal plane instead of the pupil plane, although a similar problem occurs in the focal plane: all light enters the filter under a small angle because of the focusing of the beam, but the effect is less severe and at least it is constant over the field. Two slots are available for the narrow band interference filters right after the focal plane. One of the disadvantages is that the beam has a diameter of 112 mm in the focal plane, so the common 50 mm, 63 mm, and 76 mm filters still vignette the FoV a lot.

The optical design of ACAM is shown in figure 10. Lens 1 nearly collimates the light beam to produce a pupil plane close to filter wheel 2. The beam is not perfectly collimated: it diverges slightly. There are no optical elements between lens 1 and the filter wheels box. The two parts are connected with a cylinder with a rugged and black painted inner surface. The cylinder was meant to contain a baffle but at the moment of construction this was considered unnecessary, so the baffle has not been produced.

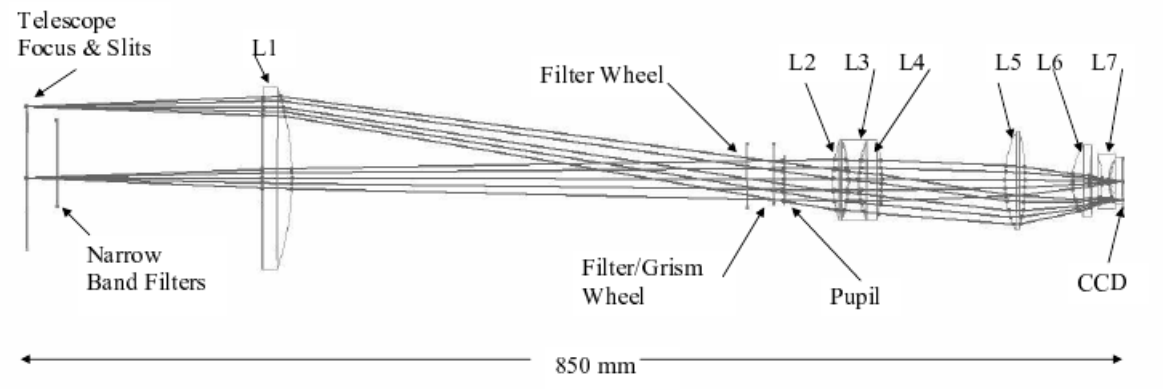

Figure 10: Optical design for ACAM [1].

After the cylinder comes the filter wheel box with two wheels. The grism is located in the second wheel, so that it is closest to the pupil plane. The filter wheels can be taken out of the instrument through one of the two doors on the side. This is useful when many filters need changing. The frequently used filters, the Sloan ones, are mounted permanently. All others can be taken out of their mounts to make room for other filters. After the filter wheels, light passes through the lenses 2 till 6 which are all placed in the same mount. Lens 7 is the final lens which also acts as cryostat window.

This section was a general overview of the WHT and ACAM. Next sections discuss the specific issues that needed solving.

3 Transmitted Wavefront Distortion of filters

3.1 Introduction

When ACAM is in imaging mode, some filters produce bad image quality. This was more or less expected because the filters were not specified to have a low Transmitted Wavefront Distortion. In order not to waste telescope time on bad filters, it is necessary to predict the performance of a filter on forehand. So a measuring setup is required to test and characterise filters off-sky. If these measurements predict the image quality well, the results are made public to observers.

A wavefront distortion is caused by the filter not being completely flat. The filter surfaces are curved slightly because of the way the anti-reflection coating was applied, or it contains scratches or other irregularities. Usually the distortions are no problem when the filter is placed in the focal plane. All light from an object in the sky is focussed on one point on the filter which is regarded as locally flat. In ACAM, however, the filters are placed in the pupil plane, and as a result the light beam from one object goes through a large area on the filter. The diameter of the beam of an on-axis source is 34 mm on filter wheel 1 and 36 mm on filter wheel 2. The smallest filters have a diameter of 50 mm, so almost any irregularity in the filter surface introduces aberrations in the final image.

There are different ways to measure the wavefront distortions introduced by optical elements. Commonly used methods are interferometry tests and Shack-Hartmann tests. In an interferometry test the distorted wavefront is combined with a flat wavefront into one beam. Interference between the two wavefronts causes fringes, from which the shape of the distorted wavefront can be deduced [9]. This method is expensive because it requires precise optics which do not distort one of the wavefronts too much; if the distortion, introduced by the optics, of one of the wavefronts is more than one λ, no unique reconstruction of the aberration in the optics can be made [5].

An alternative for the interferometry method is the Shack-Hartmann setup [8]. A flat wavefront goes through the optical element to be tested, a filter in our case, and gets distorted. The distorted wavefront passes through a lenslet array, a two dimensional array of small lenses, which focuses the light on a detector. A completely flat, undistorted wavefront will result in all spots being well focused and equally distant from each other (see figure 11). In practice they will be shifted a little, and from these positions the slope of the incoming wavefront is determined. Aberrations in the optics of the Shack-Hartmann setup are also included in this measurement, but they can easily be removed by making a calibration without the filter. This method does not demand extremely precise optics and good Shack-Hartmann sensors are

available. It was therefore used to measure the aberrations in the filters[1].

The Shack-Hartmann setup contains a few lenses to regulate the size of the beam. First the diverging beam from a small light source has to be collimated, and the resulting collimated beam should have a size similar to that of the filter. In our case this means a beam with a diameter of 50 mm. After the beam passes through the filter, the beam diameter is decreased to match the size of the lenslet, which is 5 mm (see also figure 12 for a picture of the setup). The lenslet and detector are accompanied by software to analyse the results. It displays the spots on a computer screen, reconstructs the wavefront, and fits Zernike polynomials to the wavefront. The Peak-to-Valley (PV) and Root Mean Squared (RMS) values of the reconstructed wavefront are given as an indication of the deviation from a flat wavefront. The PV is a pessimistic number as it does not take into account over how large an area the measurement was taken. Instead the RMS is a better indication of the whole filter quality.

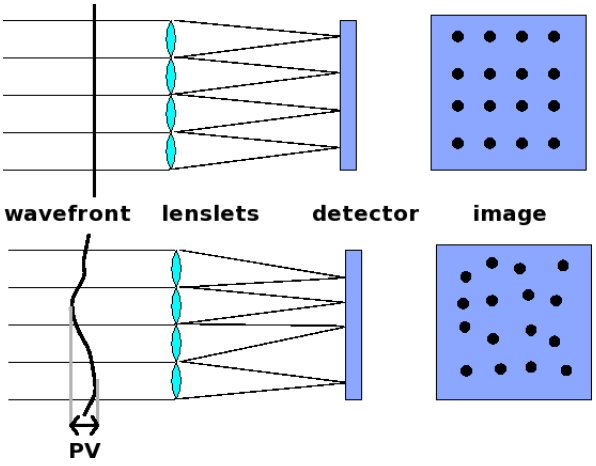

Figure 11: Principle of Shack-Hartmann sensor. Above: flat wavefront, below: distorted wavefront.

3.2 Setup

The first setup contained two light beams: one from a white light source, and one from a laser. A beam splitter directed both beams through the filter, but note that only one light source is used at a time. The final wavefront is detected by the Shack-Hartmann sensor, which consists of 39x31 small lenses focussing spots on a detector. The software which goes with the sensor reconstructs the wavefront and fits Zernike polynomials to it.

[1]The Shack-Hartmann sensor was bought from Thorlabs. Its product number is: WFS150-7AR

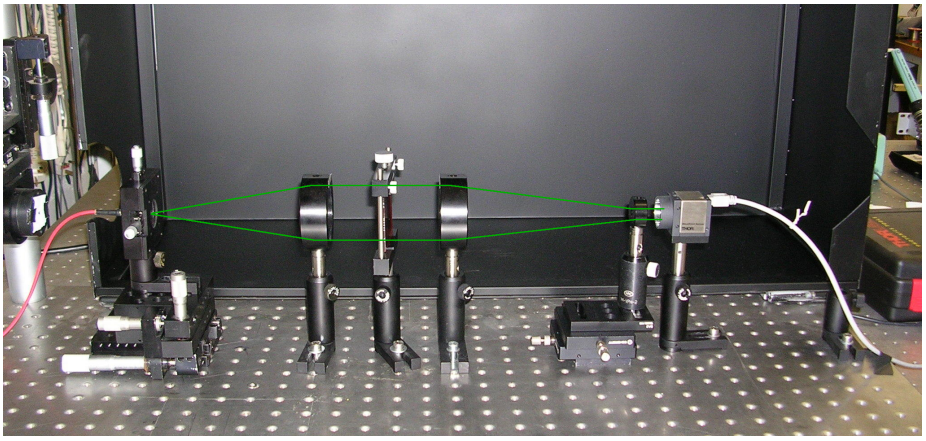

Figure 12: Picture of the final Shack-Hartmann setup with one light source only. The light enters the setup on the left through a fibre, the rest of the light path is marked by green line.

Zernike polynomials are a set of orthogonal functions that completely describe an optical wavefront distortion, each order corresponding to one of the well known optical aberrations. Table 1 lists the first 15 terms. The first three Zernike Polynomials - piston, tip, and tilt - are not included in the final measurement because they do not affect image quality. The RMS of each Zernike polynomial indicates how apparent the optical aberration is. Quadratically added and square rooted, they give the total RMS Transmitted Wavefront Distortion (TWD) of the wavefront. RMS TWDs can be given in nanometres, but it is more convenient to give them as a fraction of λ, the wavelength of the wavefront. A broad-band filter does not transmit one λ only, so in our case the central wavelength of the filter is taken. The reason for expressing the RMSes in central wavelengths is that it facilitates comparison of the filters: the for wavelength corrected RMSes relate directly with the Strehl intensity ratio for RMSes as small as $frac\lambda 14$, and good approximations exist for RMS $< \frac{\lambda}{4}$ [11]. Many filters, however, have a larger RMS TWD, and moreover not the Strehl ratio but the FWHM of the psf will be used to distinguish between good and bad filters. So although one cannot predict an exact relation between RMS/λ and FWHM, they are expected to relate better than if the RMS TWD would not have been scaled to wavelength.

ACAM has mounts for filters with diameters of 50, 63 and 76 mm. All 50 mm and most 63 mm filters were measured in both the laser beam and the white light beam, if possible. The laser has a wavelength of 633 nm, so blue filters cannot be measured with the laser. Comparison of the results from the laser and white light source showed that they differ a lot, as shown in figure 13. The reason could be that the intensity of the laser beam is not

mode	order	Norm	Zernike polynomial	Name (Thorlabs)
1	0	1	1	piston
2	1	2	$r \cdot \sin(\theta)$	tilt x
3	1	2	$r \cdot \cos(\theta)$	tip y
4	2	$\sqrt{6}$	$r^2 \cdot \sin(2\theta)$	astigmatism 0/90
5	2	$\sqrt{3}$	$2r^2 - 1$	defocus
6	2	$\sqrt{6}$	$r^2 \cdot \cos(2\theta)$	astigmatism +- 45
7	3	$2\sqrt{2}$	$r^3 \cdot \sin(3\theta)$	trefoil x
8	3	$2\sqrt{2}$	$3r^3 \cdot \sin(\theta) - 2r \cdot \sin(\theta)$	coma x
9	3	$2\sqrt{2}$	$3r^3 \cdot \cos(\theta) - 2r \cdot \cos(\theta)$	coma y
10	3	$2\sqrt{2}$	$r^3 \cdot \cos(3\theta)$	trefoil y
11	4	$\sqrt{10}$	$r^4 \cdot \sin(4\theta)$	tetrafoil x
12	4	$\sqrt{10}$	$4r^4 \cdot \sin(2\theta) - 3r^2 \cdot \sin(2\theta)$	sec. astigmatism x
13	4	$\sqrt{5}$	$6r^4 - 6r^2 + 1$	spherical aberration
14	4	$\sqrt{10}$	$4r^4 \cdot \cos(2\theta) - 3r^2 \cdot \cos(2\theta)$	sec. astigmatism y
15	4	$\sqrt{10}$	$r^4 \cdot \cos(4\theta)$	tetrafoil y

Table 1: The first 15 Zernike polynomials from the Malacara system with names according to the Thorlabs manual. The names for higher order terms, like trefoil and tetrafoil, can be different, depending on the author. A normalisation factor equalizes the RMS's of the Zernike polynomials for a unity circle.

constant enough over the whole 50 mm aperture. It showed peaks and dips: this can cause problems in the SH sensor, which will not detect enough bright spots. Only the bright spots are included in the wavefront fitting, which makes the laser light measurements unreliable. Moreover only red filters could be measured with the laser, so for a good comparison of the whole filter set a white light source is necessary. The laser source and the beamsplitter were removed from the setup and only a white light source has been used in the final setup.

The new setup was ready in February 2011. Test measurements showed that the new setup gave different results from before. Apparently the defocus terms had changed. The reason is that the optical elements in the setup introduce chromatic aberrations. Before any measurement is done, a calibration has to be made to get rid of aberrations in the setup itself. During this calibration all the white light is detected by the SH sensor, but which part of the spectrum does the SH software take for the calibration? When the red light is better in focus, the calibration is made in the red. When then a blue filter is measured, the chromatic aberrations of the SH setup are added to the measurement. Probably the first setup was optimised for the red (calibrations were done with the red part of the spectrum), while the second setup was optimised for the blue. To solve this inconsistency, all filters had to be measured again. This time a second filter, with the same

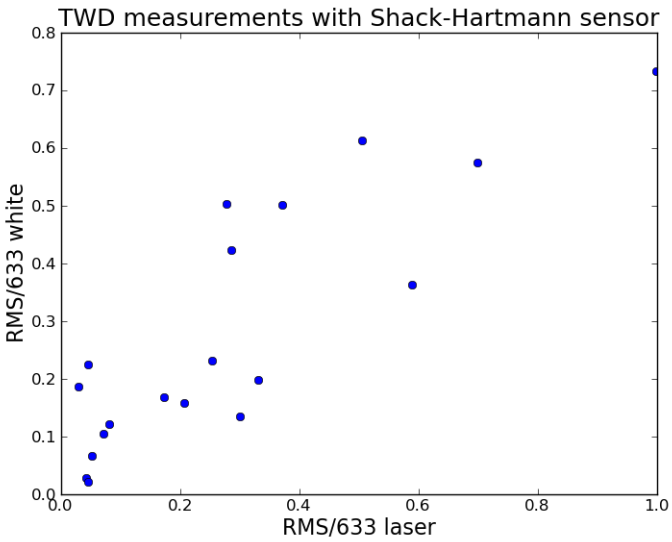

Figure 13: Measured RMS of laser and white light sources in old setup (September 2010 - February 2011) No error bars are given because the measurement error had not been investigated yet, but the differences are too large to be explained by measurement errors alone. Data can be found in Appendix A.

colour of the measured filter, was placed in the beam during calibration. These calibration filters are simply broad band filters from the WHT filter set (Harris and RGOZ). They are:

1. HarB for 380-490nm
2. HarV for 490-560nm
3. HarR for 560-730nm
4. HarI for 730-850nm
5. RGOZ for 850-950nm

U is not included in the table, because the white light source (A Stellar Net SL1 tungsten source) is not bright enough in the U-band for measurements. Also the throughput of the SH setup drops rapidly in the U, so U-band filters have not been measured.

Doing measurements by hand always introduces some errors. A series of test measurements indicates how big this error is:

- Three filters were measured ten times in a row to test the consistency of the setup. Every time the filter was taken out of the holder or turned around. Sometimes the software was restarted, or the SH sensor cable

reconnected. The three filters are: a normal broad band V filter (#51), a Taurus filter with low RMS TWD (#136), and a bad Hα filter (#73). Of the 10 measurements the RMS/633nm are respectively: 0.01, 0.018, 0.016. The (max-min)/2 for these three filters are: 0.013, 0.025 and 0.031. From these results an error of 0.03 RMS/633 nm has been adopted.

- Another uncertainty arises in the magnification of the beam, which should be 10. The placement of the lenses is not perfect and this introduces an error in the magnification. An aperture of 40 mm placed in the filter plane resulted in a beam size on the detector of 3.9 mm. Another aperture of 22 mm was projected on 2.3 mm. From this it is concluded that:
  filter=(10 $\cdot$ detector) $\pm$ 1 mm.

- Chromatic aberrations of the setup, as mentioned before, introduce errors as well. A calibration in the same wavelength area as the filter solves this partly, but the R-band is still 170 nm wide and the setup defocus changes rapidly in the B-band. A Zemax model of the SH setup shows the expected aberration as function of wavelength, as displayed in figure 14. Defocus is the dominant aberration in this plot, spherical aberration plays a minor role. Of course the theoretical model does not necessarily resemble the actual alignment. Therefore the model has been modified until its wavelength dependent defocus terms corresponds to those of the real setup. To be able to do so, one needs to know the actual defocus terms of the setup for different wavelengths. These are retrieved from two measurements for a B, I, and R filter; once with a calibration in the same wavelength area as the filter, and once with a blank calibration without any filter. The difference between these two values is the chromatic aberration introduced by the SH setup. The measured errors and the Zemax predictions are given in table 2.

  Figure 14 makes clear that especially measurements in the blue are sensitive to chromatic aberration in the setup. We assume that a calibration is made in the centre of the B-band, so at 440 nm. Zemax gives the error at the edges of the B-band, which we will take to be 410 nm and 490 nm because there are no B-band filters with $\lambda < 410$ nm. This is a pessimistic estimate of the error, but fortunately the errors are only large for the defocus terms, not for other aberrations.

An overview of all errors is given in table 3. Other possible sources of errors were eliminated: a box placed over the setup avoids turbulent air which would manipulate the measurements, and the light source is left to stabilise for about 10 minutes before using it.

Measured	Calibration	Δ Defocus	Corrected for wavelength	Zemax
44(I)	43	-1.476	-1.174	-1.27
43(I)	44	-1.483	-1.179	
39(R)	37	0.519	0.522	0.523
37(R)	39	0.638	0.642	
26(B)	25	-0.015	-0.022	between -2.67 and 0.85
25(B)	26	-0.079	-0.116	

Table 2: RMS TWD measurements to characterise the chromatic defocus of the SH setup. Column 1: the measured filter, 2: the calibration filter. 3: the difference in defocus term between the measurement with, and without calibration filter. 4: the same as 3 but now corrected for central wavelength. And 5: the predicted defocus term by Zemax. As one can see from the table and the plot in figure 14 the correlation is not very precise but sufficient to get an impression of the error in the defocus term of our SH setup.

Filter	Defocus (setup)	Spherical (setup)	Measurement	Spherical+measurement
B(440 nm)	3	0.4	0.04	0.4
V(530 nm)	0.5	0.15	0.04	0.16
R(650 nm)	1	0.13	0.03	0.13
I(790 nm)	0.7	0.01	0.02	0.02
Z(900 nm)	0.5	0.01	0.02	0.02

Table 3: The different errors, in units RMS/central wavelength, for a 40 mm aperture on the filter. The Defocus and Spherical are the maximum errors one can expect from the Shack-Hartmann setup itself. The last column is the total error, excluding the error in Defocus. The reason is that users do a focus run when putting in a new filter, so the error in the defocus measurement should not be of importance when picking a suitable filter for observations. Moreover the large errors in the defocus terms would make the final measurement meaningless, since these are usually below 0.5λ.

3.3 Results

In March 2011 all 50 mm, 63 mm and 76 mm filters in the WHT have been measured, except for the U-band filters and a very red filter because they had too low throughput for a good measurement. In total 147 filters have been measured, each one twice: once with a 25 mm aperture and once with a 40 mm aperture. The 40 mm aperture measurements are used in all tables and figures because they are a better measure of the overall filter quality. Appendix A contains a table with the filter number, defocus term, and the total RMS TWD with and without defocus term. Part of the data has been compared with observations. Figure 15 shows the measured defocus term related to the applied telescope defocus in mm. The data comes from focus runs on different nights. There is one outlier, which has a large astigmatism term. Astigmatism is an off-axis aberration and is therefore important if it

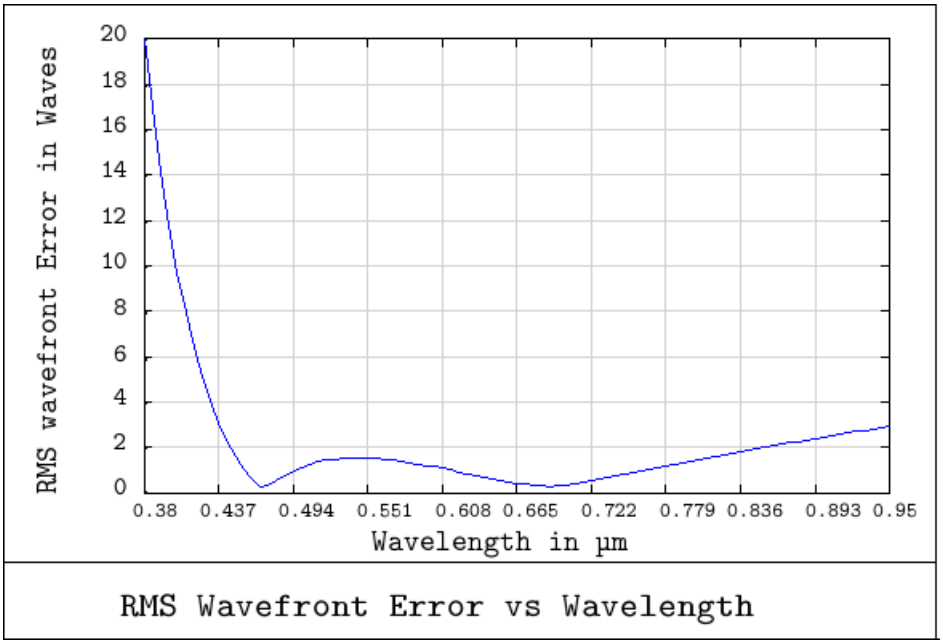

Figure 14: Chromatic aberration in new SH setup (February 2011). The total RMS is the sum of defocus and spherical aberration.

is very large and the star is not completely on axis. Because it blurs the image it is difficult to find the best telescope focus, so the measurement is unreliable. The other measurements show a clear relation between telescope defocus and measured defocus RMS TWD, a least squares fit of a straight line gives: offset = 0.0816·SHrms + 0.011. The filter measurements are a good prediction of the telescope defocus that has to be applied.

Other aberrations than defocus cannot be corrected for, so a decision has to be made on how large a RMS TWD is still acceptable. Pinhole experiments showed the result of placing a filter in one of the filter wheels in ACAM. First a pinhole is placed in the instrument's focal plane, and no filter in the filter wheel. It produces a spot, smaller than 1 by 1 pixel, on the detector. A filter in the filter wheel distorts the image and increases the FWHM of the spot. The experiment was done during the day with top ring lights on. The difference with real observations is that seeing is not apparent here. For the rest all aberrations introduced by the telescope, instrument, and filter are included, so the experiment it a good approximation to what happens during observations at night. It has been a bit selective though: only r and H-alpha filters were used. The reason is that other filters would produce spots out of focus. Since ACAM does not contain a focus mechanism itself, the pinhole must be placed exactly in the focal plane. The position of this plane depends on wavelength, and the pinhole could only be placed at the right position

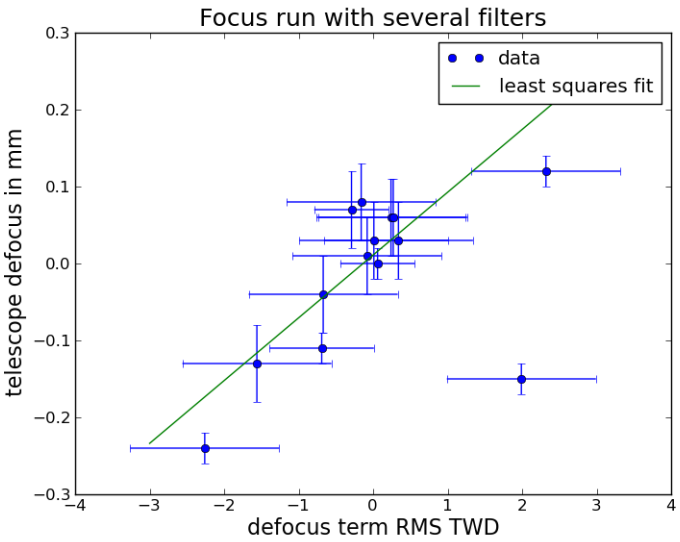

Figure 15: Telescope defocus retrieved after a focus run. The errors on the x-axis are taken from table 3, and the telescope accuracy was 0.05 or 0.02 mm, depending on the night. The outlier can be explained by its large astigmatism, making it difficult to determine the best telescope focus. The least squares fit (offset = 0.0816·SHrms + 0.011) does not take this outlier into account.

for red light. As one can see in figure 16 there is a clear relation between measured RMS TWD and the FWHM of the produced spot. Filters with an RMS up to 0.5λ are projected on less than one pixel, which corresponds to 0.25 arc second. A filter with RMS $< 0.5\lambda$ is therefore supposed to be a good one. 84% of the filters are good, according to this criterion, if the defocus term is not included in the measurement. Even with defocus term included 59% of all filters remain. This high percentage is mainly because of the large set of narrow band Taurus filters which are specified to have low RMS TWD.

After the measurements, new Sloan filters with RMS TWD $< 0.25\lambda$ over a 1 inch aperture were ordered. Sloan g, r, z, and i filters arrived within the same year, a Sloan u filter within specification had not been found before the end of the year. All data are available to the ING staff through the internal filter database. Observers can find a summary on the ACAM web page.

3.4 Conclusion

The RMS TWD of almost all filters that can be used in ACAM has been measured with the Shack-Hartmann setup and a white light source. These

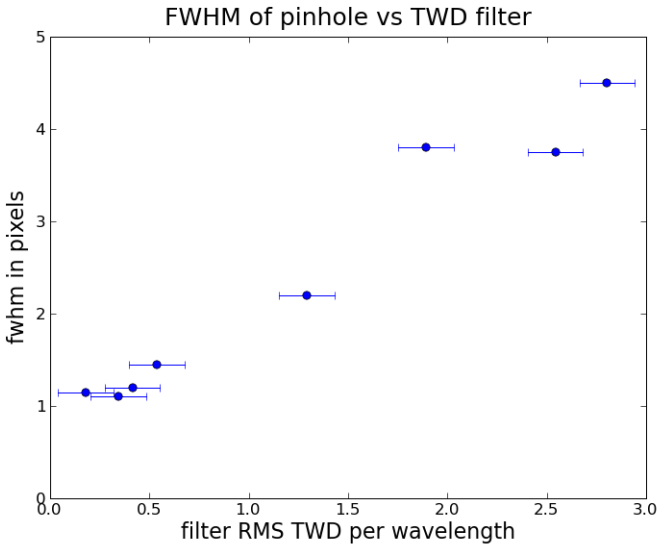

Figure 16: Results from the pinhole experiments. The FWHM is never smaller than 1 pixel since that cannot be fit. From the plot it is concluded that filters with RMS $< 0.5\lambda$ still give FWHM of the psf of less than a pixel. The pixel size of the ACAM detector is 0.25 arc second.

RMSes correlate well with the FWHM of the projection of a point source on the detector. A filter with RMS $< 0.5\lambda$ still results in a spot with FWHM of less than a pixel, so less than 0.25 arc second. This is the case for 59% of all 147 filters, and if the defocus term is not included in the measurement it applies to 84% of the filters. (For individual results, see appendix A.) Because some filters contain high defocus terms, it is wise to do a separate focus run for every filter used during an observation. One can correct well for defocus but not for any of the other aberrations. Moreover the measured defocus term can contain large errors, so these values should be used with caution.

4 Scattered Light

4.1 Introduction

Already during the commissioning of ACAM a scattered light problem[2] arose. The scattered light is clearly apparent for observations between 4 and 30 degrees from the moon. It degrades the image quality and therefore eliminating it has high priority.

Observations with ACAM in imaging mode show scattered light as in figure 17: an exposure with the moon between about 4 and 30 degrees from the telescope. The affected area is about 2 or 3 times as bright as when it would not be affected. When the moon is 'above' the telescope, so at higher elevation, the light falls on the upper part of the ccd. This symmetry remains, independent of telescope pointing and moon position. The pattern on the ccd changes slightly with moon position, but covers in general half of the ccd. Obviously this is a problem for observations during bright time, but also during dark time scattered light may get into ACAM, although from another source, like planets or bright sky. The problem with scattered light from a bright sky is that it affects the flat fields. If this happens indeed, we do not only have a problem during bright time, but any time when good flat fields are required, for example when precise photometry has to be done.

4.2 Effect on flat fields

Whether the flat fields are severely affected or not can easily be ascertained observing a crowded field with bright stars. The magnitudes are retrieved twice from the exposures: once from the flat fielded images, and once from the non flat fielded images. These then are compared to known magnitudes. Magnitudes from SDSS are accurate enough for this purpose: the error is 0.01 mag for bright stars ($<$ 16.3 SDSS magnitude), which we plan to use.

The night of the observations was not photometric, the FWHM of the stars' psf varied from 6 to 12 pixels. Fortunately the FWHM stayed between 6 and 8.5 pixels during most exposures, so only these were used. In total three fields were observed: SA101, SA104 and SA107. SA101 was observed at low elevation (airmass 2.2) and the transmission seemed to vary from exposure to exposure so these data were omitted. The data from SA104 and SA107 were reduced with IRAF, and the magnitudes determined with IRAF's package noao-digiphot-apphot-phot. The size of the aperture around the stars has to be chosen carefully to get accurate results. Too large an aperture will include too much background, which increases the error in the

[2]From the beginning the problem got the label 'scattered light' although we did not know yet what the light scattered off. A more general and therefore correct term would be 'stray light'.

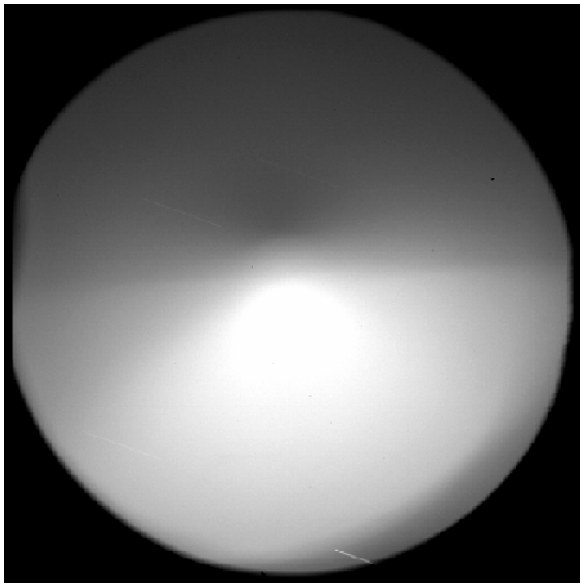

Figure 17: Typical scattered light pattern in ACAM in imaging mode, when observing between 4 and 30 degrees from the moon.

magnitude. A small aperture, on the other hand, will exclude some of the star light. The amount of excluded star light depends on FWHM of the psf of the star. Since the FWHM slightly varies from star to star, the aperture must be large enough not to distinguish between a FWHM of 6 and 8.5 pixels. An aperture of 30 pixels turned out to be the best compromise: the difference between a magnitude retrieved from a 30 and 35 pixel aperture is < 0.01 mag, and the error given by PHOT is also < 0.01 mag (for stars with magnitude < 14.5 by IRAF, and < 16.3 for SDSS).

Still there could be transmission variations from one exposure to another. One can only tell whether this is the case by comparing the difference between SDSS magnitudes and observed magnitudes from exposure to exposure. In the ideal case this is a constant close to 0 if telescope and instrument transmission are accounted for. It would be a problem if the variation between exposures is much larger than the variation between stars on the same exposure, since in that case data from different exposures cannot be compared. This is fortunately not the case: the difference in magnitude between the exposures is as large as the difference in magnitude between stars on a single exposure. The introduced error is 0.01 mag, which is added to the total error.

Figures 18 and 19 show the difference between observed and SDSS magnitudes as function of radius from the ccd centre. The difference is not 0 because telescope and instrument throughput have not been corrected for,

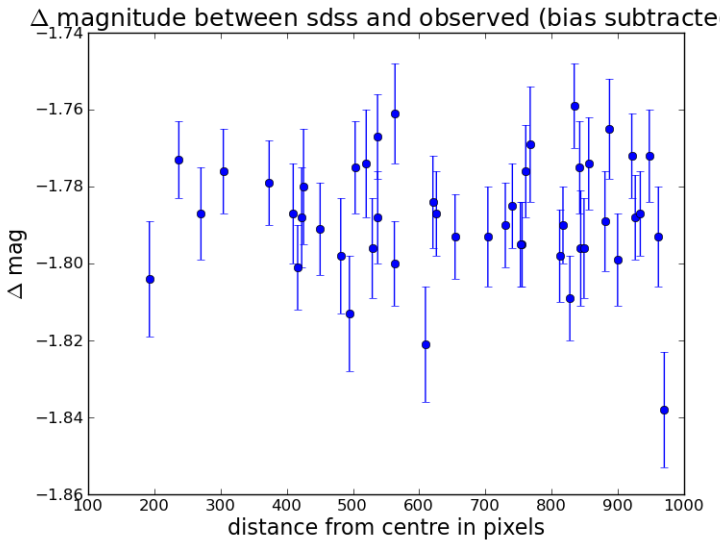

Figure 18: The differences between SDSS magnitudes and our calculated magnitudes for the fields SA104 and SA107 for the bias subtracted exposures. There is no obvious relation with the distance from the centre. The outlier was probably too close to the edge of the field.

but we are only interested in the scatter. The first plot, which has only been bias subtracted, shows no clear relation with distance to ccd centre, and the range is 0.079 mag. There is one outlier, possibly because this star is on the edge of the field. If this point is omitted the spread becomes 0.062 mag. On the other hand the flat fielded data does show an almost linear relation, and the spread is almost twice as large: 0.109 mag. Because the spread is smaller for non flat fielded exposures, the photometry is more accurate in those images. Apparently flat fielding has a degrading effect on the image. We now know the effect of the scattered light on ACAM, but not yet on the other instruments.

ACAM is the only instrument which shows scattered light so prominently, but this does not necessarily mean that the other instruments do not suffer from it at all. With a large FoV and no baffling around the focal plane, ACAM is extra sensitive to off-axis light, so scattered light will show up here first. Another explanation is that there is a light leak in ACAM itself or in the A&G box. The question to be answered is thus: "What path does the moonlight take before it arrives at the ACAM ccd?". Only once this is clear a proper solution can be provided.

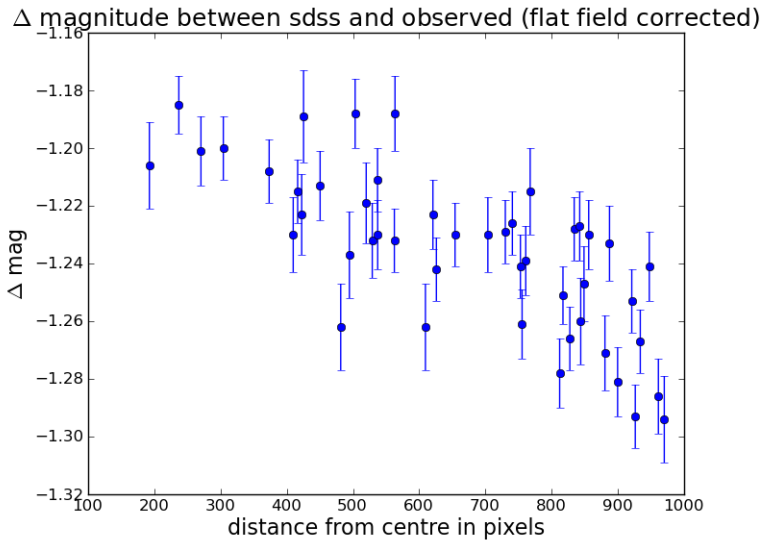

Figure 19: The differences between SDSS magnitudes and our calculated magnitudes for the fields SA104 and SA107. This is for the flat fielded data. A relation between Δmag and distance from centre of the ccd can be seen, suggesting that the flat fields are not really flat, thus affecting the photometry.

4.3 Revealing the light path

For over a year tests have been performed in order to find the light path taken by moonlight. Especially in the beginning all tests had to be done on-sky. Only a few nights every month are available for technical issues and service proposals with any of the instruments at the WHT, so the tests started up slowly. The first results are summarized below:

- Moonlight scatters off something close to the primary mirror, and not off the secondary mirror (or the construction around it). This was tested with the moon close to zenith. Scattered light was visible on ACAM images while the dome shutter was completely open. Then the dome shutter was closed with small steps. One could see clearly from inside the dome which parts of the telescope were lit by the moon and which not. The scattered light disappeared from the images while the secondary mirror was still bathing in moonlight and the primary was completely shaded from moonlight.

- Yet the primary mirror does not reflect the moonlight itself. When the mirror petals are closed, the scattered light is still visible and has the same pattern as before. This means that the moonlight has to scatter off something else than the primary mirror.

- The secondary mirror is not a part of the light path taken by the moon-

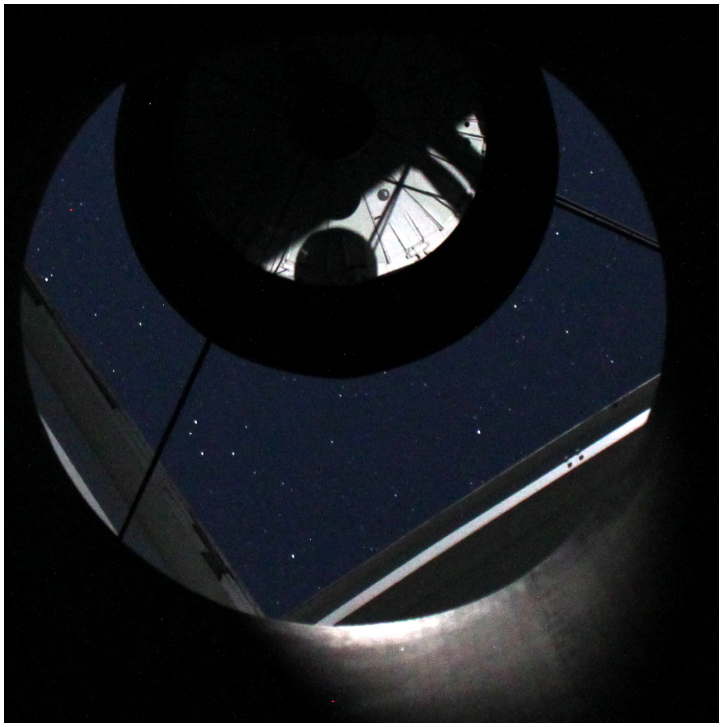

Figure 20: Picture taken from the Nasmyth turret in the direction of the secondary mirror. A bright spot is visible on top of the sky fog baffle. From this picture the primary mirror seems to reflect moonlight in the direction of the secondary mirror too. This is probably not the cause of the scattered light, since the mirror petals were closed when the picture was taken to allow the photographer to stand on them. Moreover this picture is just a hint in the right direction: we can not directly derive the intensity of the scattered light on the ccd from it.

light. For one test the secondary mirror was covered in a black cloth, for another test the secondary mirror was not even at the telescope. In both cases the scattered light pattern was visible in ACAM.

- One more test restricts the possible light paths further: ISIS is probably also affected by scattered light. When scattered light was visible with ACAM, the ISIS slit view showed a strong gradient. This means that the problem applies to Cassegrain instruments, and possibly all instruments. It has not been noted before as clearly as with ACAM, because most instruments do not accept much light coming in off-axis.

A different approach finally revealed the light path. Pictures were taken from the inside of the telescope during an ACAM D-night (D from Discretionary time, during which technical tests are performed). See figure 20 for a picture taken from inside the Nasmyth turret. A bright spot shows up in the sky fog baffle. It suggests that moonlight enters the telescope through this baffle

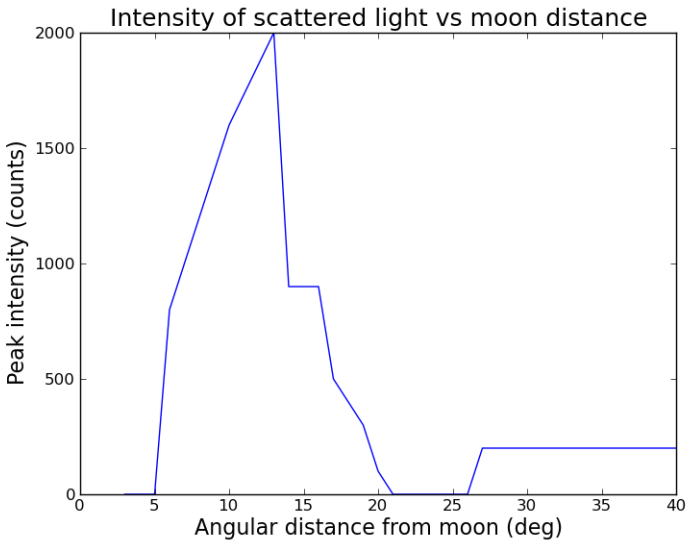

Figure 21: Intensity of scattered light as function of moon angle.

which does not absorb it sufficiently. Also it explains why the primary and secondary mirror do not play a role in the scattering. To make sure that this is indeed the main source of scattered light, another test was performed to find the role of the Nasmyth holes. Two exposures were taken: one with the moon illuminating one of the Nasmyth holes, and one with the moon illuminating the covered Nasmyth hole (there are 3 open holes and one covered hole in the Nasmyth turret). The pattern and intensity of the scattered light did not change, so the Nasmyth holes do not play a significant role.

Another interesting, and confirming, result is given in the plot in figure 21. It shows the intensity of the scattered light as function of moon distance from the telescope pointing in degrees. The intensity in this plot is the peak intensity in the image (usually in the centre) minus the background. Of course this intensity is not constant from night to night, since it depends on moon phase, but the shape of the plot is always the same. At 4 degrees the scattered light starts to appear in the images, at 13 degrees the intensity reaches its maximum. There is a dip between 21 and 26 degrees. Around 27 degrees the light reappears but at this level it is not problematic any more. Figure 22 explains the observed pattern. At 13 degrees the moon is not blocked by the secondary mirror baffle any more, it goes straight into the sky fog baffle and Nasmyth turret. From 22 degrees the top end flip ring and the top end ring start to cover the moon. At about 35 degrees the moon appears completely from behind these rings, but because of the

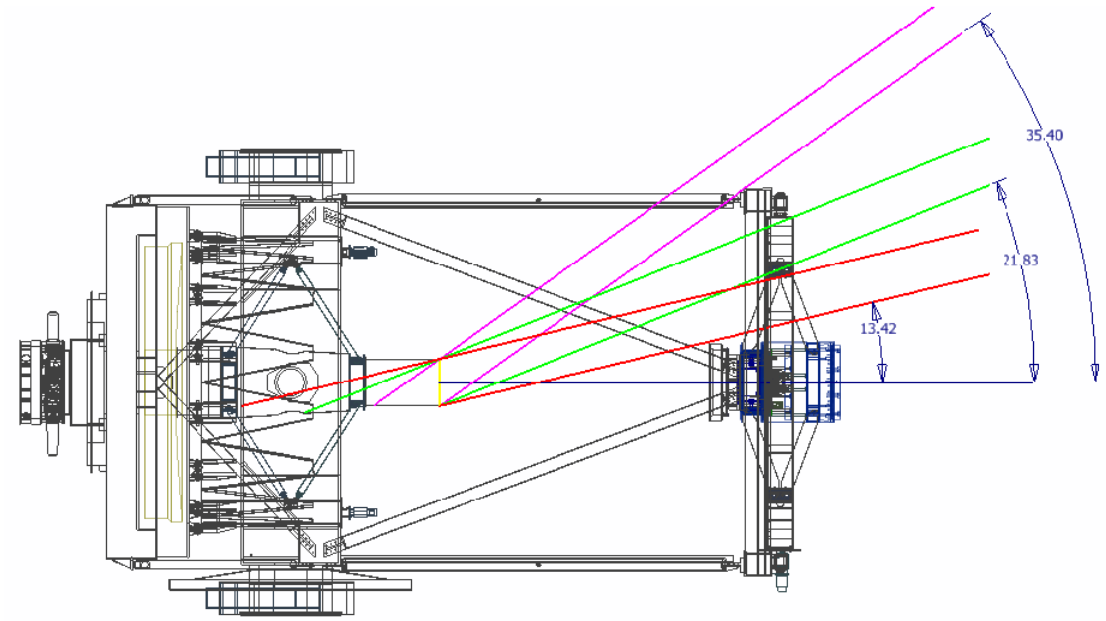

Figure 22: The moon illuminates the entire inside of the sky fog baffle and Nasmyth turret when it is 13 degrees from telescope pointing.

high angle it only illuminates a small part of the sky fog baffle. The small amount of light intercepted by the sky fog baffle has to reflect multiple times now before making it to ACAM. It is thus expected that the intensity of the scattered light is lower.

The most obvious solution is turning the sky fog baffle into a light-trap baffle. The sky fog baffle and the Nasmyth turret baffle are black painted cylinders just wide enough for the autoguider to observe. The black painted surfaces absorb up to 90% of light falling on it[3], the rest is reflected and scattered. One reflection from such a surface would thus allow 10% of the moonlight to continue to the instruments: a lot of light during bright time. A common solution is a light-trap baffle, this is a series of rings which 'trap' the light. No light entering the telescope through the sky fog baffle can be reflected directly to the ACAM fold mirror in the A&G box.

A simple light-trap baffle was produced, consisting of flexible tubes which were taped into a cylinder that just fits in the sky fog baffle. (For an overview

[3]We don't know exactly how much light is absorbed because many different black coatings exist each with their own properties. An indication for the amount of absorbed light by a standard coating is given by Avian Technology [13]

of all measures of the sky fog baffle and the Nasmyth turret, see appendix B.) The cylinder was 1130 mm long, the tubes had a diameter of 40 mm and were cut in half to give them flat surfaces. These half tubes were taped into the cylinder with their flat surface facing the sky and a distance of 60 mm between them. With this ratio 40:60 all light that falls in the baffle with an incident angle below 34 degrees should be trapped. That night, however, the scattered light on the ACAM images was worse than the night before. Different explanations are: the moon was waxing, the baffle was too short to have a significant effect, or the tubes reflected light back to the secondary mirror. Moreover the tubes were so big that they vignetted the autoguider so it would not have been a permanent solution.

4.4 Zemax simulations

In order to better understand which parts of the telescope and instrument play an important role in the scattering process, simulations can be done with a ray tracing programme like Zemax. The advantage of simulations is that solutions can be investigated, and no material or observing time is wasted on trying these out.

In order to simulate the scattered light in Zemax, it is necessary to have a good model of the telescope. There are detailed mechanical models of the WHT which can be imported in Zemax, but ray tracing then takes a very long time. Different from before, Zemax is now used in Non Sequential Mode. In Non Sequential Mode the rays are traced from object to object instead of from surface to surface (the front page of this report shows what this looks like). Objects can reflect, scatter, and absorb light rays. Both specular reflection and scattering are interesting since we do not know yet how moonlight makes it from the sky fog baffle to the ACAM ccd. The conditions for the ray tracing could be that every ray hitting an object is split in a reflected ray and 10 scatter rays. Furthermore the minimum amount of starting rays is 10^6, otherwise there will not be enough detections on the ccd to recognise a pattern. If it takes four scatters before the intensity of the ray is too small to consider, there is an enormous amount of rays to be traced. And possibly this is not yet enough. Figure 23 shows the result for 10^7 starting rays, which does not resemble the pattern we see on the ACAM ccd. Because all details of the telescope are modelled it takes hours to days to run a simulation.

The discrepancy between simulated and observed pattern on the ccd suggests that the simulation is not precise enough. One of the reasons could be that ACAM and the A&G box are not included in the telescope model, so the optical parts are added to the model separately. Lens barrels, internal structure of the A&G box and internal surfaces of ACAM are therefore

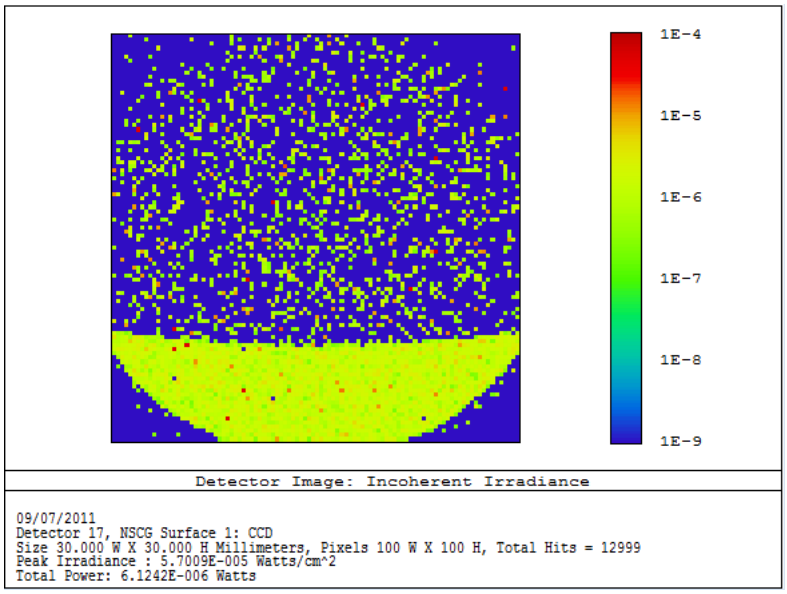

Figure 23: Result of a simulation with Zemax where the whole telescope has been imported. This was for a source at 12 degrees, ten million rays, and all surfaces scattering 80% and reflecting 20% of the incident light. The ray tracing took 1-2 days.

excluded from the model even though they could play an important role in the scattering process. Another problem lies in the assignment of surface properties to different parts of the telescope. Because the telescope has been imported as one part, only one set of properties can be assigned to the whole surface (like: 80% of the light is scattered and 20% is reflected). Importing all parts separately hardly helps because we don't know how much light is absorbed, scattered and reflected by every single surface. Nor do we know the type of scattering. It can be Lambertian, scattering in all directions, or Gaussian. In the simulations Lambertian scattering has been assumed, which should be a good approximation for rough surfaces. Because of all these uncertainties and the long time it takes to try things out, a simpler model is more appropriate.

The simplified model reduces the turret and baffle to cylinders, and omits the rest of telescope. The ray tracing goes much faster, as was expected, but the detected pattern looks completely different again. Although this new model is not expected to be more accurate than the original one, it allows at least try outs within a reasonable time; absorbing or reflecting rings can be added on the position of ACAM barrels to find their importance. The cylinder between Lens 1 and the filter wheel in ACAM, which was supposed to contain the baffle, affects the scattered light significantly, according to this simplified model. An ACAM baffle might reduce the amount of scattered light arriving

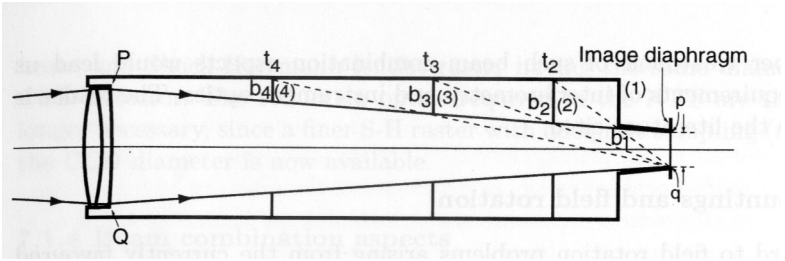

Figure 24: Image copied from Wilson's *Reflecting telescope optics 2*. It shows the design of a light-trap baffle around the science beam with extremes Pp and Qq.

at the ccd, but by how much can not be predicted from the Zemax model: we do not know how much light is currently reflected/scattered by the cylinder. Second we do not know how correct the simplified model is. So although the simulations give some feeling for what happens inside the telescope, the outcomes are not reliable enough to provide a confident solution.

4.5 Alternatives for simulations

An alternative for Zemax is simulating the moon by shining a torch into the sky fog baffle. This proved to produce the same pattern on the ccd as the moon does. Later a lamp with a small angle beam was used instead of a torch to better approximate the far away moon. The lamp was attached to the dome to obtain a fixed position with respect to which the telescope could move. This way off-sky tests were done to predict the effect of some test baffles. In the case that a test baffle does not remove the scattered light off-sky there is little reason to expect that it will do so on-sky. The argument does not work the other way around; if a baffle removes scattered light off-sky it does not guarantee the working of it on-sky. The lamp produces a beam much smaller than that of the moon, so it illuminates a smaller part of the telescope. So a baffle that eliminates scattered light from our fake moon has to be tested on-sky as well.

We started the lamp tests with a cardboard light-trap baffle in ACAM. Its design is based on figure 24 from Wilson's *Reflecting Telescope Optics 2* [10]. P and Q are the edges of a lens, similar to Lens 1 in ACAM. The extreme field rays are Pp and Qq where p and q can be regarded the edges of a filter in the filter wheel. Now the first step to take, according to Wilson, is making the smaller tube at the end of the cylinder which leads to pq. We will not do that because the filter wheel has to move freely. Instead an aperture is made on the end of the cylinder which is just large enough to let the science beam through. A line, drawn from the edge of the filter (q) through the edge of the aperture (b_1), determines the place of the next aperture (t_2). This process is repeated up to the end of the cylinder. With

Figure 25: Cardboard ACAM baffle which consist of five parts with in total eight apertures.

such a baffle all light that enters the cylinder through the lens (PQ), but leaves the science beam, is intercepted by an aperture. Ideally the baffle is as long as the cylinder between Lens 1 and the filter wheel box (296 mm) to be as effective as possible. But this is complicated because the baffle has to be inserted through an opening in the filter wheel box, which is only 100 mm wide. So the baffle cannot be inserted in one piece: there must be three pieces at least, which should connect easily so that they can be assembled in the dark by someone balancing on stairs.

The strategy explained above resulted in a cardboard test baffle for ACAM. The baffle consists of 5 parts with in total 8 apertures. A picture of the final result is given in figure 25. In spite of the careful design and production it was still difficult to get it in ACAM completely. Finally only four parts with in total five apertures were inserted. Although not complete it should show some improvement. The results from the lamp test are plotted in figure 26 and show that the ACAM baffle reduces the scattered light level by 20% at most. This is not enough to call it a solution.

In addition to the ACAM cylinder, also Lens 1 may help stopping the scattered light. It is a large piece of optics close to the focal plane and scattered light could reflect from the lens edges. Therefore a black cardboard aperture, with a diameter of 120 mm, was added on the focal plane side of Lens 1, to prevent any stray light from scattering inside the lens. It probably does not

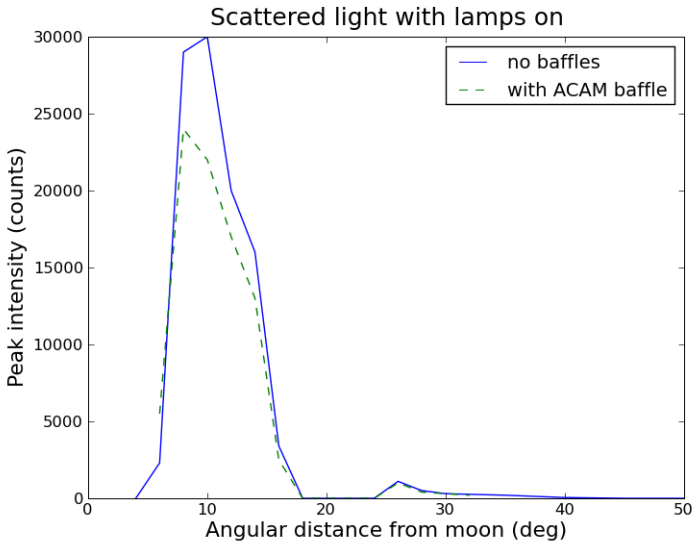

Figure 26: Scattered light level in counts from a lamp set to 100 volt. Exposures of 0.5 second are taken with the ccd 4x4 binned.

reduce the scattered light by much but it does not vignette the science beam either so it was left in ACAM. The cardboard baffles were tested on-sky the same night but the outcome was the same as for the lamp tests. In addition another on-sky test was performed with a ring placed on the bottom of the sky fog baffle. Different from the light-trap, this ring has a smaller aperture and consists of one piece only. The first ring had an aperture of 530 mm, and when that showed no improvement a second ring with aperture of 400 mm was tested. Again this hardly showed any change.

The ACAM baffle was expected to work because it would intercept all scattered light outside the science beam. It is powerless to do anything about light that follows the science beam. Is this the reason that the ACAM baffle helped so little? Earlier a test had been performed to investigate something slightly different, with the goal to find whether scattered light came in through the centre of the focal plane or not. Apertures with different diameters were placed in ACAM's focal plane, and an exposure was taken. A surprising result was that no scattered light was detected outside the clear FoV of the aperture. If scattered light would reflect somewhere in ACAM it could end up over the whole ccd. Instead the scattered light pattern abruptly stops at the edge of the aperture. See figure 27 for the results of a 100 mm and 40 mm aperture in the focal plane. In each case the bright parts are clearly restricted to a certain aperture. So the scattered light follows the science beam in ACAM and must therefore be removed before it reaches ACAM's focal plane.

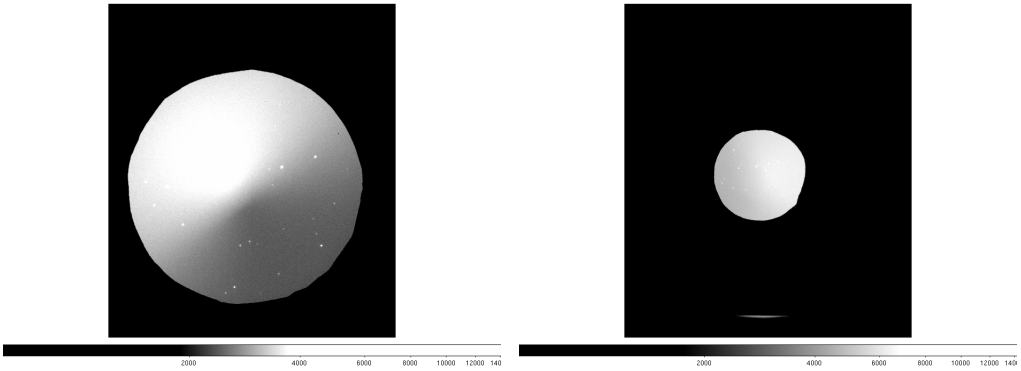

Figure 27: Left: exposure with a 100 mm aperture in the focal plane and the Sloan r filter in filter wheel 2. Right: a 40 mm aperture in the focal plane and again Sloan r in filter wheel 2. The pointings are different because the moon moved between the exposures. This may explain why the illuminated area switched side. Support astronomers at the WHT say to have seen this happen as well after filter changes or when another neighbouring filter is placed in the filter wheel, but this has never been confirmed. Note that the scattered light pattern is restricted to the aperture which was placed in the (first) focal plane of ACAM.

4.6 Telescope baffles

The situation has left us nothing else to do than baffling the telescope itself. Most parts of the telescope are hard to reach and therefore we should avoid placing baffles there. A few places are accessible: the sky fog baffle can be removed to place something in it, and also the space under the Nasmyth fold mirror is within reach. One then has to climb on the mirror petals, reach through a Nasmyth hole, and be very careful not to drop anything inside the telescope which then falls in the A&G box and damages the optics. Designing a baffle is not as straightforward as pictured by Wilson in figure 24 this time, because it is not clear what the analogies for the optics are.

So instead Autodesk Inventor, an Autocad-like programme, was used to decide which parts should be baffled. One can 'walk through' the telescope model looking from the inside out. By highlighting a part of the telescope it is at once clear which surfaces see this part. Apparently the tube from the Nasmyth fold mirror sees the sky fog baffle and the sky. The most obvious solution is baffling the turret tube although it quickly starts vignetting the autoguider. Finally 4 black cardboard rings were placed in the turret. They vignette the autoguider and ACAM significantly, but let enough light go through to notice a reduction of the scattered light. In addition we made a sky fog baffle according to figure 28, and ACAM still contained the baffle and aperture in front of lens 1 from the night before. During the night, the

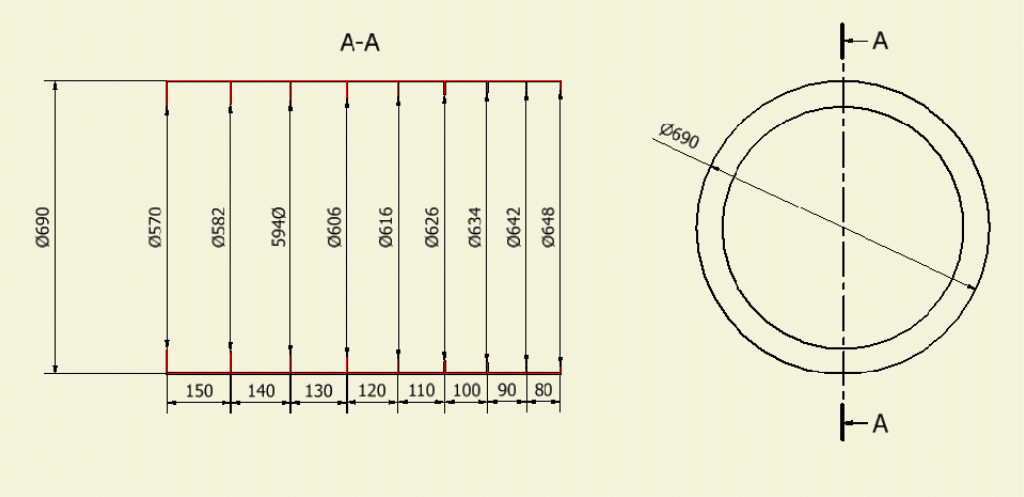

Figure 28: Design of the light-trap baffle to be inserted in the sky fog baffle. Right facing the sky, left facing the instruments. Designed by Kevin Dee.

baffles were removed one by one to see what difference they make to the scattered light intensity. The results are plotted in figure 29 and printed in Appendix C. The sky fog baffle reduces the intensity of the scattered light by 40%, and the turret baffle eliminates it completely. Two things should be noted here: In the exposures with the ACAM and L1 baffle the background is only 4.000 counts as opposed to 10.000 for 10 degrees and this has not been explained. Second the turret baffle vignettes ACAM's field by about 10% at the edges. So scattered light intensities less than 10% of the background may not have been noticed.

The light-trap baffle in the Nasmyth turret was most successful in eliminating the scattered light, but it vignettes ACAM and the autoguider so it needs to be redesigned. Alternative ways of baffling exist, these are worth investigation now because they may solve the vignetting problem. New materials are available which absorb $> 99\%$ of the incidence light. Simply covering the inside of the telescope therefore seems a good solution. After contact with Acktar [12], a company that produces these materials, it was decided to go for the 'old-fashioned' type of baffle with rings. The absorbing material is too expensive to cover the whole telescope with, and moreover too delicate and perhaps not durable enough for the changing weather conditions. The new baffle design for the Nasmyth turret is shown in figure 30. It still vignettes the edge of the autoguider up to 30%, so when the baffle is installed it must first be tested that this causes no problems for guiding. This appeared to be no big problem: the vignetting is less than 10% for the part of the autoguider field that is actually used. The new baffle has been made of plastic and is permanently placed in the Nasmyth turret. It

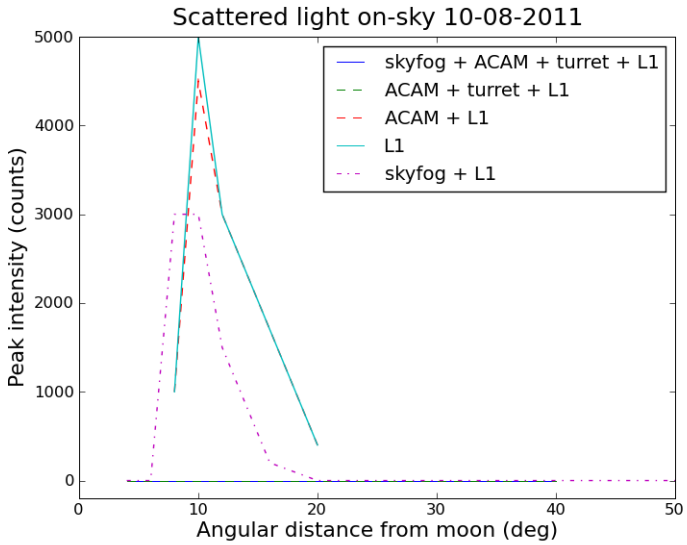

Figure 29: Amount of scattered light with the use of different baffles. The new sky fog baffle reduces it by 40 percent. The turret baffle eliminates it but also vignettes the ACAM FoV so cannot be used permanently.

removes 70% of the scattered light intensity. Although an improvement, it still is an unsatisfactory solution. The next step is probably the addition of a light-trap in the sky fog baffle, but that will unfortunately happen after this writing.

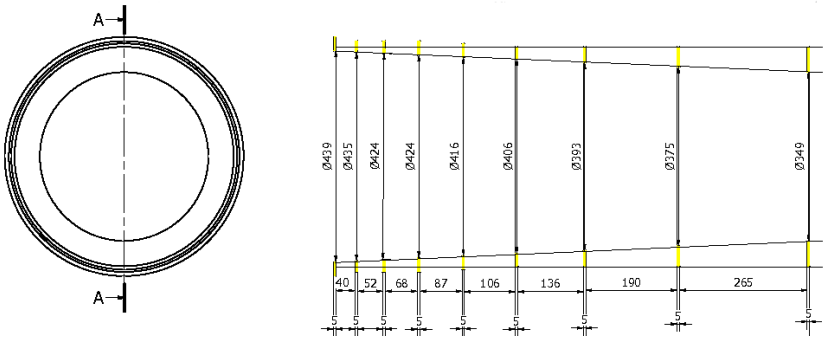

Figure 30: The final baffle to be placed in the Nasmyth turret. The largest aperture (439 mm) faces the sky, and is located at 3520 mm from focus. Design by Kevin Dee.

4.7 Conclusion

Scattered light in the WHT affects not only ACAM but also other instruments at Cassegrain focus. They suffer less than ACAM, which is with a large opening in the focal plane extra sensitive to scattered light. For ACAM there are two consequences: during bright time about half of the ccd has a background 2 to 3 times higher than the rest of the ccd. Second the flat fields are not flat irrespective of presence of the moon. As a result of the latter, observations for photometry are better not flat fielded.

The light enters the telescope through the sky fog baffle, and is reflected or scattered inside the Nasmyth turret. This happens most efficiently when the moon is 13 degrees from telescope pointing because moonlight then illuminates the whole inside of the sky fog baffle and Nasmyth turret. An attempt to simulate the scattering process in Zemax was not successful. It is possible to include a model of the whole telescope in Zemax, but ray tracing takes hours up to days in that case. Moreover the scattering and reflecting properties of all the surfaces in the telescope are not known.

After some experiments with cardboard baffles we partly managed to remove the scattered light from ACAM exposures. The intensity has been reduced to 30%, at the cost of 10% extra vignetting in the autoguider field, and this was accomplished by a light-trap baffle in the Nasmyth turret. A light-trap baffle in ACAM was not successful: the intensity was reduced to 70 % and improvements are not expected because the scattered light follows the science beam in ACAM. Scattered light therefore has to be removed before reaching ACAM's focal plane. Quite possibly the final solution will consist of a few 'light traps' in the telescope, for example one in the sky fog baffle and one in the Nasmyth turret.

5 Grism design

5.1 Introduction

As mentioned in the section on Telescope and Instrument design, the filter wheels in ACAM can contain a dispersing element to turn ACAM into a spectrograph. A Volume Phase Holographic (VPH), comparable to a transmission grating, is already available for this purpose [3]. The VPH needs the light to enter under a specific incidence angle for which it was optimised (the blaze angle), and the spectrum leaves the VPH under some angle as well. A VPH thus bends the light path, and this is not desired. Two prisms are required to bring the light path back to straight: one on either side of the VPH. These two prisms had to be designed, ordered, and attached to the VPH. Once the VPH assembly (also called grism) arrives, it is tested and mounted in ACAM.

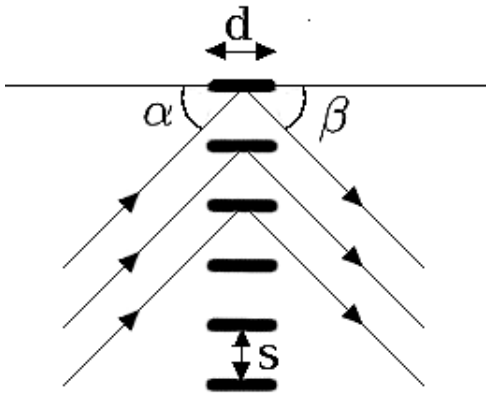

Figure 31: Simplified VPH: α is the angle of incidence, β the angle of refraction.

The dispersing part of a VPH is a transparent layer in which the refractive index n is not constant but modulated. The planes with higher index are called fringe planes. The plane density is one of the properties of the VPH and is usually represented by the letter v, with the units fringes/mm[4]. Figure 31 shows the principle, with instead of v here $s = \frac{1}{v}$: the spacing between the fringes. VPHs work according to the same principle as normal (surface relief) gratings, so the grating formula can be applied:

$$mv\lambda = \sin(\alpha) - \sin(\beta). \tag{4}$$

[4]Often the density is given in lines/mm, because the width of the plane, d, is small compared to its length.

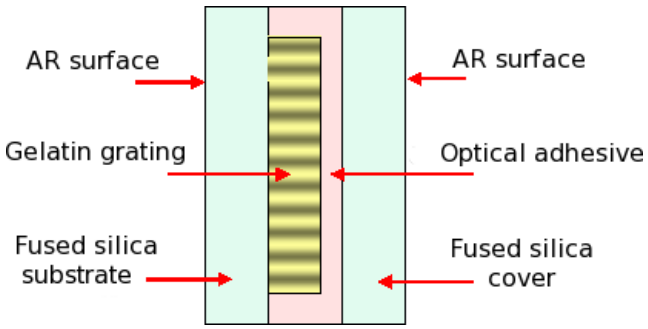

Figure 32: Parts of VPH with anti-reflection coating.

where m is the order of diffraction, λ is the wavelength in nm and v in fringes/nm. α the angle of incidence and β the angle of diffraction. However, a VPH is a volume whereas a grating is a surface. So a VPH has an additional parameter: the thickness of the layer d. This thickness is typically a few to a few hundred microns. Because of the thickness the diffraction is dominated by the Bragg effect [4]. The Bragg effect is the interference which occurs when X-rays are sent through a thin piece of crystal with layers of atoms. Constructive interference occurs whenever $mv\lambda = 2\sin(\alpha)$ (so the incidence angle equals the outgoing angle), with $\frac{1}{v}$ the distance between the atom layers. The VPH is an enlargement of the atomic crystal: this time λ is larger and the line density is smaller. So instead of the grating equation (4) we will use Braggs law (equation 5) with $\alpha = -\beta$.

$$mv\lambda = 2\sin(\alpha). \tag{5}$$

Braggs law suggests that for any incidence angle there is only one diffracted wavelength per order m. In practice β is a range around $-\alpha$, and accordingly a range of wavelengths around the Bragg wavelength is emitted. This range of transmitted wavelengths, or bandwidth, is determined by Δn and d. With these parameters a VPH can be optimised for one specific wavelength or for a wavelength range.

A VP grating as described above is usually made using holographic techniques, hence the name Volume Phase Holographic. A photosensitive layer of dichromated gelatin is coated onto a piece of glass. This layer is exposed to two interfering laser beams, making a wave pattern in the gelatin. The wavelength of the laser light and the angle between the beams determine the fringe tilt and the fringe density v. The gelatin needs wet processing to obtain the desired properties: the longer the gelatin is placed in the liquid bath, the more prominent becomes the modulation in index Δn. When it has the desired properties it is sandwiched between two glass plates. The result is a durable and easy to handle VPH, because the glass protects the gelatin layer and can be touched and cleaned. See figure 32 for an example.

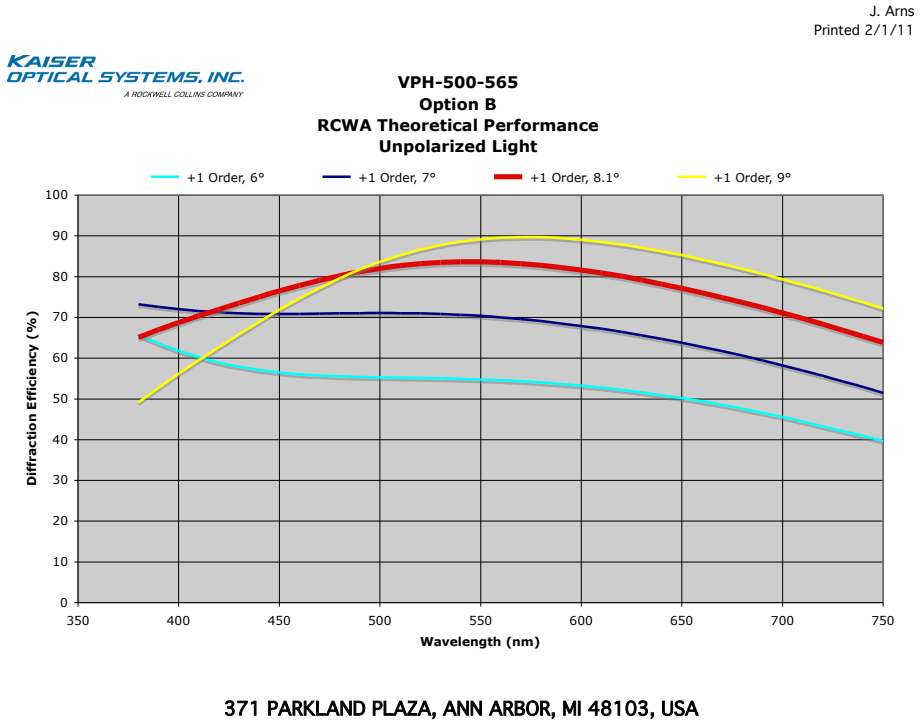

Figure 33: Diffraction efficiency for the new VPH as function of incidence angle in air.

As mentioned before the VPH has a certain blaze angle. Other incidence angles will still produce a spectrum, as long as they do not differ too much from the blaze angle, but the diffraction efficiency of the VPH changes. The new VPH to be mounted has been optimised for the range 500-565 nm for an incidence angle of 8.1 degree in air (in practice the VPH is not embedded in air but in silica in which the incidence angle is 5.4 degree). For this angle, however, the diffraction efficiency of the VPH falls off quickly in the blue, meaning that little blue light goes into the first order. The efficiency in the blue increases for a smaller incidence angle, but this should not be taken too far because the VPH is not optimised for this incidence angle and the overall throughput decreases. Figure 33 shows the effect of incidence angle on the diffraction efficiency. Angles between 6 and 7 degrees clearly favour the blue, but the overall throughput in the red decreases.

The grism already available in ACAM contains a 400 lpmm VPH. It has a wavelength resolution of 1.3 nm for a 1 arcsecond slit. Although this VPH works well, an additional 500 lines/mm VPH has been purchased to meet

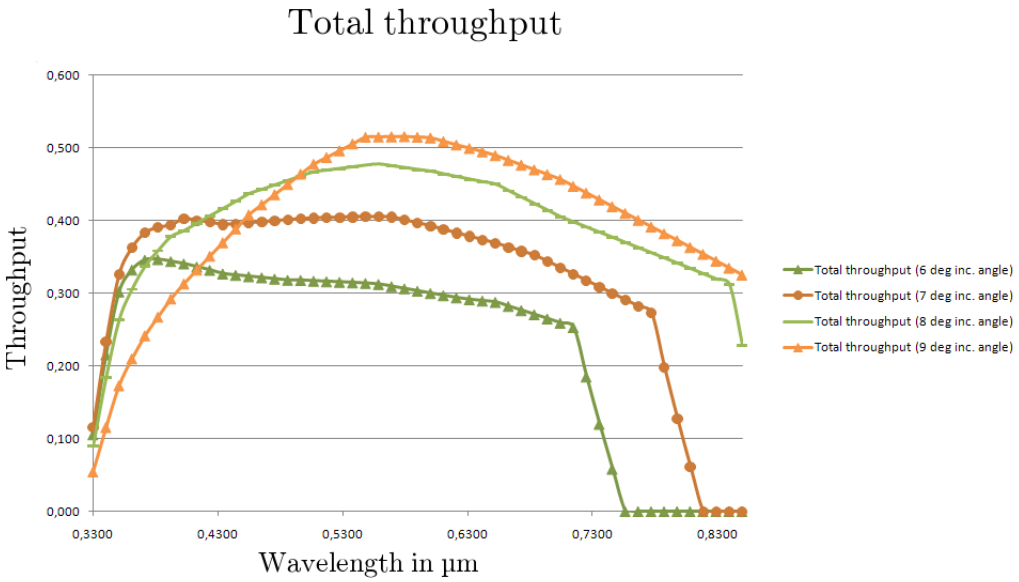

Figure 34: Total throughput of telescope + ACAM + grism for different incident angles (in air) on the VPH.

the requests from the astronomy group: the grism containing the new VPH gives higher resolution because of the increase in lines/mm, and the prisms should be designed to give better throughput in the blue.

5.2 Prism design

Our task is to design a prism that bends the straight beam to the desired incidence angle upon the VPH. There are a few restrictions on this angle: first of all, the VPH needs to be efficient at this incidence angle. Diffraction efficiency of the new VPH varies a lot between 6 and 9 degrees. But also the throughput of the telescope and ACAM is important: at 330 nm the throughput goes to 0. Figure 34 plots the total throughput of telescope, instrument and grism for different incident angles on the VPH.

The prism that bends the light by the desired amount has two variables - prism angle and material - that are optimised for spectral resolution. The spot sizes are ideally smaller than a resolution element, how large the resolution element is depends on the slit width. We take a 1 arcsecond slit, which is projected on 4 pixels or 60 micron. Zemax can do the optimisation once it knows what the variables are and what needs to be optimised. The variables are the kind of glass and the prism angle (see figure 35 for a VPH with a prism and the prism angle). The choice for the kind of glass was simple: there are only a few possibilities because the prisms needed ordering soon and only BK7 (name as used in zemax), N-SF57, and flint glass (N-LAK9)

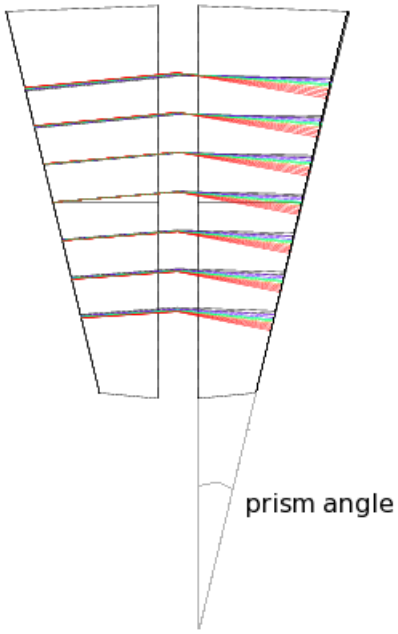

Figure 35: A grism with rays traced from an on-axis source. Image from Zemax.

were available in a short time. Because of this limited choice we simply optimised once for every glass separately, although it is also possible to include all glasses available in the Zemax catalogue in the optimisation. Important properties of the glass are: refractive index, abbe number, throughput and price. The refractive index should be high in order to bend the incoming beam efficiently. If not, the low n has to be compensated for by a larger prism angle, which makes the grism too long. Moreover the refractive index should vary little from blue to red, so $\frac{\Delta n}{\Delta \lambda}$ should be small. Abbe numbers are a measure of this wavelength dependence, and are given in Zemax as: $\frac{n_d - 1}{n_C - n_F}$ where d,C and F are Fraunhofer lines of He(587.6 nm), H(656.3 nm) and H(486.1 nm) respectively. Larger Abbe numbers are favoured as they imply less variation in n as function of wavelength. The main properties of the glasses are listed in table 4.

glass	n	Abbe nr	relative price	λ range
BK7	1.5168	64.167	1	310-2325 nm
N-SF57	1.846	23.78	4	370-2500 nm
N-LAK9	1.691	54.71	5	320-2500 nm

Table 4: The most important properties of the glasses that were readily available from the manufacturer ICOS.

The main variable in the optimisation is prism angle. The two prisms will be identical so that the spectrum is centred around the Bragg wavelength. One has to indicate in Zemax for which wavelengths the optimisation needs to be done, and whether all have the same weight or not. This was not at once clear from the specifications, which were 'good throughput in the blue and an as large as possible wavelength range'. So four different wavelength ranges have been studied: intermediate range (380-750 nm), blue (330-700), red (380-850) and total (330-850). The wavelength ranges were chosen this way because the 380-700 nm range is not so sensitive to changes in prism angle, while the ranges 330-380 nm and $>$ 700 nm are. Also we need to specify whether optimisation has to be done for on-axis sources only, or for a whole range of field angles. The slit covers in principle a 7 arcminutes strip on the sky, but optical aberrations increase the spot size for off-axis sources, and thus decrease the resolution. We do not want to give up resolution for on-axis sources in an attempt to optimise for resolution on the whole field. So during the optimisation process only the fields with 0, 0.384 and 0.762 arcminutes radius are included.

The resulting spot sizes for the total wavelength range (330-850 nm) and for different incidence angles onto the VPH are given in figure 36. BK7 was taken as glass because the aberrations introduced by the three glasses were so small that it did not make any difference in spot size, and BK7 is the cheapest glass. Note that the smaller incidence angles result in higher resolution in the blue, but that some vignetting appears in the red. This vignetting is caused by lens 5, 6, and the cryostat window because they are not big enough to intercept the reddest part of the spectrum. The throughput plot in figure 34 shows the same cut off in the red. Based on figure 36 it was decided to let the incidence angle be 7.5 degree in air, which corresponds to 4.94 degrees in BK7, and this is accomplished by making the prisms with an angle of 13.708 degree. The blaze wavelength is 504 nm and the resolution of the new grism is 1.03 nm/4 pixels in the blue and 1.09 nm/4 pixels in the red (this is the average resolution for the range 330 - 540 nm and 540 - 800 nm. They are not equal because resolution is not completely linear).

5.3 Grism performance

The manufacturer of the prisms assembles the grism and applies anti-reflection coatings to it. After arrival of the grism a few tests have to be performed, in order to check throughput, dispersion, and size. Throughput is tested by shining a laser beam through the grism and compare the intensity with a photometer to that of an undisturbed beam. For $\lambda = 633$ nm the throughput is 85.5% and this is slightly better than specified: 86% (throughput vph at 633 nm) * 0.99 (-1% for coated surfaces) = 84.3%. The dispersion is found by shining the same laser beam parallel to a table onto a ruler. When

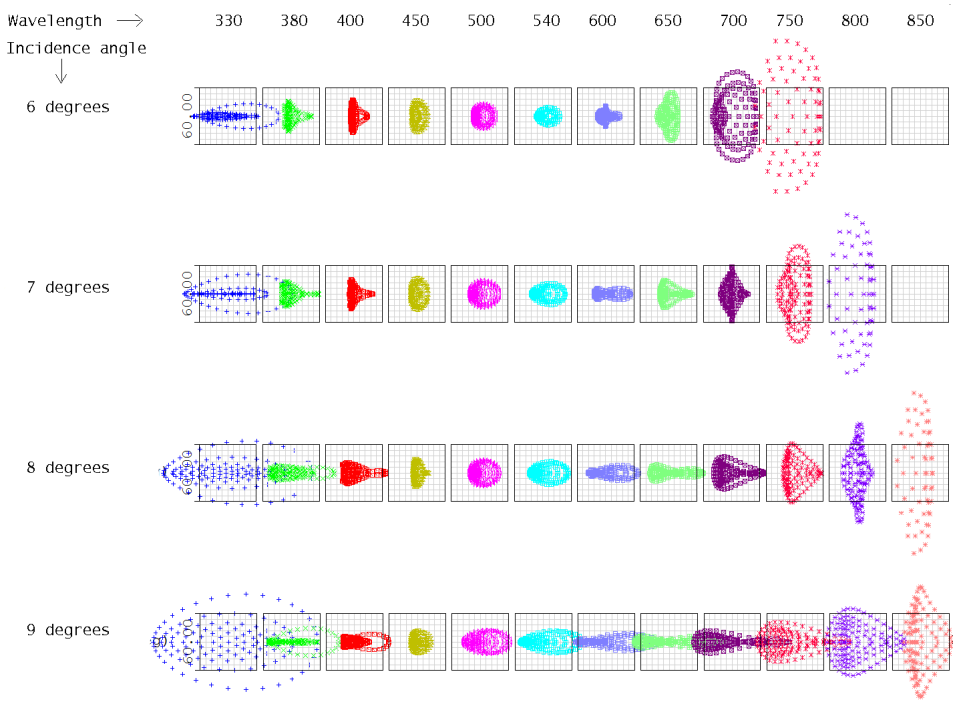

Figure 36: Spot sizes for an on-axis source with prisms made of BK7 for various incidence angles (in air) onto the VPH. The boxes have a size of 60 micron, corresponding to a 1 arc second slit. Angles of 6 and 7 degrees meet the resolution requirements in the blue, but at the expense of throughput in the red. The optimisation angles retrieved from Zemax are all between 6 and 9 degrees, for clarity the spot sizes for 6, 7, 8, and 9 degrees are given.

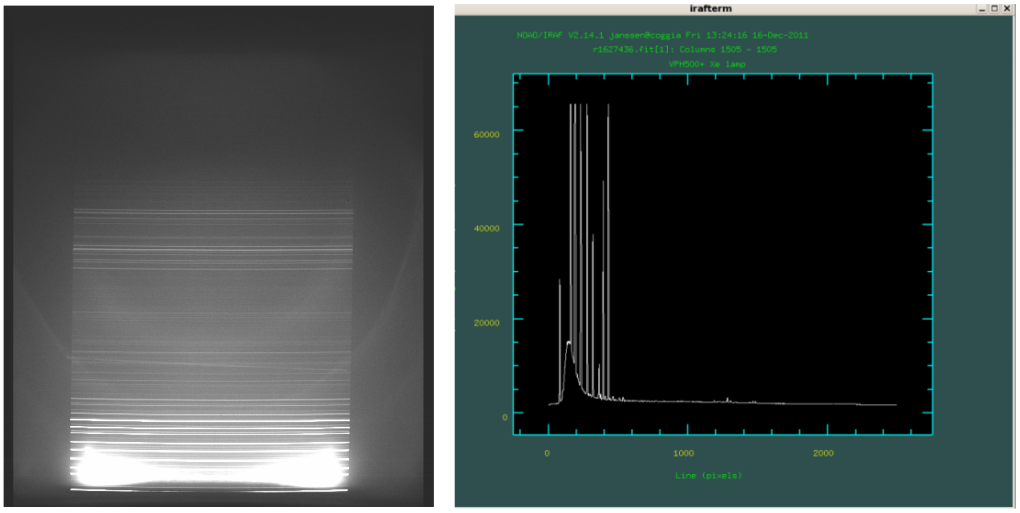

Figure 37: One of the first images taken with the 500 lines/mm grism and a xenon lamp. The spectrum shows the saturated lines and the ghost. Right: a column of the image on the left. Line 0 corresponds to $\lambda \sim 830$ nm.

the grism is placed in the light beam it bends the beam and the new position is read from the ruler. The shift was compared to a zemax model, which confirmed that the dispersion is correct. Finally the width and the heigth of the grism should be 50.00 +0, -0.1 mm, which was indeed the case.

When everything appears to be as specified, a mount for the grism is made. This mount must be sand blasted and black painted to prevent reflection off the mount, which would cause ghost images. Small screws keep the grism in place inside the mount, although there is only little margin: the grism fits tight in the mount and the alignment should be good already. One of the first spectra taken with the new grism and a xenon lamp is shown in figure 37. It is an overexposed image which clearly shows the ghosts caused by red light. Although it seems severe the intensity of the ghost is less than 10% of the intensity of the spectrum. The ghosts will become a problem when a faint spectral line is observed close to a bright line with $\lambda \sim 750$ nm. 2 masks with diameters of 45 and 39 mm on the 'sky side' of the grism did not change or remove the ghosts. The 400 lpmm grism also shows ghosts in the red part of the spectrum. Although annoying, it has not been a big problem yet. Note that the spectrum in figure 37 contains no blue lines because of the xenon spectrum.

5.4 Conclusion

Two prisms have been designed for the new 500 lines/mm VPH. They are made out of BK7 and have a prism angle of 13.708 degree. This optimises the final grism for the blue with a blaze angle of 504 nm. The resolution is 1.03 nm/4 pixels in the blue and 1.09 nm/4 pixels in the red, where 4 pixels are chosen as resolution element because this corresponds to the width of a 1 arcsecond slit. With anti-reflection coatings on the prism surfaces the throughput is 85.5% at 633 nm. A mount contains the grism permanently and can be placed in ACAM. It works as expected although there are some ghost images but this is the case for the other, 400 lines/mm, VPH as well.

6 Acknowledgements

This work has been done with the help of many people. In the first place I would like to thank Reynier Peletier, Marc Balcells and Chris Benn for letting me go to La Palma. They encouraged me to experiment and suggest new approaches, at the same time making sure I did not get stuck. Moreover I enjoyed working in the ING a lot thanks to the staff. I would like to thank especially Neil O'Mahony and Tibor Agócs for all the work we have done together, and for the time they took to explain me everything about the telescope and ACAM. I shall have a hard time trying to find colleagues with whom I enjoy working as much as with you two.

References

[1] *ACAM – a new imager/spectrograph for the William Herschel Telescope*, Chris Benn, Kevin Dee, Tibor Agócs, SPIE 70146X-1, 2008

[2] *Introduction to Volume Phase Holographic (VPH) Transmission Gratings and Applications.* An image has been used from this article, which can be found on the website of the producer Kaiser Optical Systems.

[3] *Volume-phase holographic gratings and their potential for astronomical applications*, Samuel C.Barden, Willis S. Colburn, James A.Arns, SPIE 3355:866-876, 1998

[4] *Volume phase gratings for spectroscopy, ultrafast laser compressors, and wavelength division multiplexing*, James A. Arns, Willis S. Colburn and Samuel C. Barden, SPIE 3779:313-323, 1999

[5] *Optics – fourth edition*, Eugene Hecht, 2002

[6] *Applied optics and optical engineering*, Volume 6, Rudolf Kingslake, Brian J. Thompson, 1980

[7] *Waves in layered media – second edition*, L.M.Brekhovskikh, 1980

[8] *Reflecting telescope optics 1*, R.N.Wilson, 1996

[9] *Optical shop testing*, D.Malacara, 1978

[10] *Reflecting telescope optics 2*, R.N.Wilson, 1999

[11] *Strehl ratio for primary aberrations in terms of their aberration variance*, Virendra N. Mahajan, Journal of the Optical Society of America, vol. 73, page 860, 1983

Moreover companies provided information in the form of websites, emails and catalogs. These companies are:

[12] Acktar: manufacturer of new black materials.
`www.acktar.com`

[13] Avian technologies: manufacturer of black coatings.
`www.aviantechnologies.com`

[14] ICOS: provider of prisms for the grism.
`www.icopticalsystems.com`

[15] Kaiser Optical Systems: provider of the VPH for the grism.
`www.kosi.com`

[16] Thorlabs: provider of the Shack-Hartmann sensor and black cardboard.
www.thorlabs.de

[17] Iscaac Newton Group of Telescopes: organisation where the research took place.
Offices: Edificio Mayantigo / Calle Alvarez Abreu, 70 / 2 piso / E-38700 Santa Cruz de la Palma / Canary Islands / Spain
www.ing.iac.es

A Filter measurements

The first table contains the TWD measurements with a laser and a white light source in the first Shack-Hartmann setup. The aperture on the filter was 25 mm. The measurements are RMS/633 because the laser-light has a wavelength of 633 nm. Measurements include up to the tenth Zernike mode, excluding the first three modes: piston, tip and tilt. Every filter in the ING has a number, as given in the table. The online ING filter database provides details of all filters.

nr	laser	white
011	0.504	0.613
012	0.278	0.503
014	0.173	0.168
015	0.207	0.159
030	0.371	0.501
031	0.589	0.364
032	0.044	0.224
033	0.029	0.187
037	0.254	0.232
038	0.042	0.028
039	0.046	0.022
049	0.699	0.574
050	0.300	0.136
051	0.286	0.423
053	0.998	0.733
084	0.070	0.105
176	0.051	0.066
216	0.331	0.198
233	0.080	0.122

The following table includes the final RMS of the Transmitted Wavefront Distortion of all measured filters in white light. Column 1 gives the number of the filter according to the ING database. The second column gives the central wavelength of the filter, the third the defocus term of the filter , the fourth the total RMS with defocus, but without piston, tip and tilt. The last column is the same as the fourth but with the defocus term (quadratically) subtracted. All measurements are RMS/λ where λ is the central wavelength of the filter.

nr	central λ	defocus	RMS with Defocus	RMS without defocus
8	4313	0.62	0.80	0.51
11	5326	1.11	1.23	0.55
12	5438	0.62	0.71	0.35
14	6391	0.37	0.39	0.11
15	6430	0.27	0.47	0.39
17	8113	0.03	0.11	0.11
20	8663	0.06	0.12	0.11
21	8748	-0.09	0.11	0.06
22	8734	-0.08	0.10	0.05
24	8750	-0.79	0.81	0.18
25	4296	-1.07	1.11	0.29
26	4300	-0.09	0.75	0.75
27	4304	-0.46	0.56	0.32
28	4304	0.38	0.47	0.28
30	5461	0.21	0.72	0.69
31	5452	-0.79	1.44	1.21
32	5438	0.06	0.07	0.04
33	5438	-0.05	0.06	0.03
37	6373	0.38	0.62	0.49
38	6370	0.22	0.22	0.04
39	6390	0.13	0.13	0.03
41	8120	-0.69	0.70	0.13
43	8060	-0.03	0.04	0.01
44	8095	-0.05	0.05	0.01
47	4370	-0.16	0.70	0.69
48	4385	-0.19	0.89	0.87
49	5450	0.71	0.88	0.53
50	5450	-0.54	0.62	0.31
51	5450	0.65	0.75	0.37
53	6479	2.32	2.37	0.47

nr	central λ	defocus	RMS with Defocus	RMS without defocus
55	8112	0.58	0.60	0.16
56	8112	0.12	0.49	0.47
57	8130	0.76	0.89	0.45
58	6559	1.99	4.36	3.88
61	6570	0.27	0.54	0.46
62	6553	1.15	1.56	1.05
63	6594	0.34	0.42	0.25
64	6607	-1.97	2.04	0.53
65	6626	0.01	0.18	0.18
66	6645	-1.56	1.89	1.07
67	6656	0.67	0.69	0.18
68	6686	-0.08	0.35	0.34
69	6695	1.86	3.43	2.88
71	6712	-0.08	0.31	0.3
72	6736	0.38	2.54	2.51
73	6785	-2.29	2.80	1.62
74	6834	-0.67	1.29	1.11
75	6876	0.90	1.25	0.88
76	6923	-2.26	2.42	0.85
77	6962	2.31	4.17	3.48
80	4685	0.88	0.89	0.13
81	4861	1.50	1.53	0.28
82	5009	-0.34	0.40	0.22
83	5877	0.62	0.64	0.16
84	6298	0.24	0.31	0.2
85	6584	-0.03	0.17	0.16
86	6727	-0.33	0.35	0.14
87	7331	0.72	0.72	0.05
88	9077	0	0.02	0.02
89	9540	-0.30	0.30	0.04
97	4550	0.39	0.42	0.15
98	4570	0.2	0.21	0.05
99	4770	1.13	1.14	0.08
100	4868	0.88	0.98	0.42
101	4880	1.54	1.54	0.09
102	4883	0.97	1.07	0.44
103	4898	1.02	1.10	0.41
104	4912	1.08	1.12	0.29
105	4962	-0.38	0.42	0.19

nr	central λ	defocus	RMS with Defocus	RMS without defocus
113	5033	-0.02	0.22	0.22
114	5045	-0.27	0.5	0.43
115	5052	-0.94	1.06	0.48
116	5065	-0.26	0.29	0.13
117	5072	-0.37	0.49	0.33
118	5092	-0.22	0.37	0.3
119	5111	-0.22	0.27	0.15
120	5129	-0.24	0.27	0.12
121	5145	-0.06	0.12	0.11
122	5162	-0.2	0.23	0.1
123	5175	-0.04	0.11	0.1
124	5196	-0.02	0.15	0.15
125	5214	-0.13	0.16	0.09
127	5232	-0.08	0.11	0.09
128	5250	-0.13	0.16	0.09
130	5340	0.19	0.19	0.05
133	5700	0.87	0.87	0.08
134	5905	0.75	0.75	0.08
135	5960	0.68	0.68	0.06
136	6240	0.54	0.55	0.05
137	6303	0.18	0.18	0.05
139	6565	-0.08	0.31	0.3
140	6568	-0.22	0.33	0.24
141	6577	0.42	0.56	0.38
142	6589	-0.06	0.32	0.31
143	6589	-0.14	0.76	0.75
144	6590	0.02	0.04	0.03
146	6610	-0.02	0.17	0.17
147	6613	-0.25	0.3	0.15
148	6631	-0.02	0.22	0.22
149	6637	-0.06	0.1	0.08
150	6652	0.24	0.5	0.44
151	6673	-0.14	0.14	0.05
152	6673	0.1	0.25	0.23
153	6685	-0.13	0.15	0.08
154	6689	-0.04	0.06	0.04
156	6697	-0.07	0.09	0.06
157	6709	-0.12	0.13	0.06
158	6721	-0.11	0.13	0.07
160	6733	-0.14	0.15	0.04

nr	central λ	defocus	RMS with Defocus	RMS without defocus
161	6745	-0.19	0.2	0.06
162	6757	-0.16	0.17	0.03
163	6769	-0.23	0.23	0.05
164	6770	0.05	0.07	0.06
165	6781	-0.14	0.15	0.03
166	6793	-0.29	0.29	0.05
168	6805	-0.19	0.2	0.05
169	6817	-0.19	0.19	0.05
170	6829	-0.23	0.25	0.09
171	6841	-0.22	0.22	0.04
172	6853	-0.32	0.33	0.07
173	6865	-0.25	0.26	0.08
174	6877	-0.3	0.31	0.08
175	6889	-0.28	0.28	0.06
176	6310	0.22	0.24	0.09
179	4119	-5.14	5.15	0.33
180	4710	1.21	1.23	0.22
181	5498	-0.29	0.44	0.33
182	4895	1.57	1.59	0.24
183	4879	0.74	0.85	0.41
189	4686	0.54	0.61	0.27
216	6228	0.34	0.34	0.08
217	7796	0.39	0.39	0.04
218	4844	0.45	0.45	0.05
219	4852	0.36	0.37	0.06
231	4353	0.01	0.17	0.17
232	5300	1.67	2.37	1.68
233	6450	0.4	0.41	0.1
234	8110	0.08	0.09	0.02
235	6600	-0.36	0.97	0.9
705	6390	-0.33	0.46	0.32
706	6390	0.07	0.07	0.01

B Telescope measures

The following page gives the measures of the sky fog baffle, Nasmyth turret, primary mirror, and mirror cell extension box. All measures are in mm.

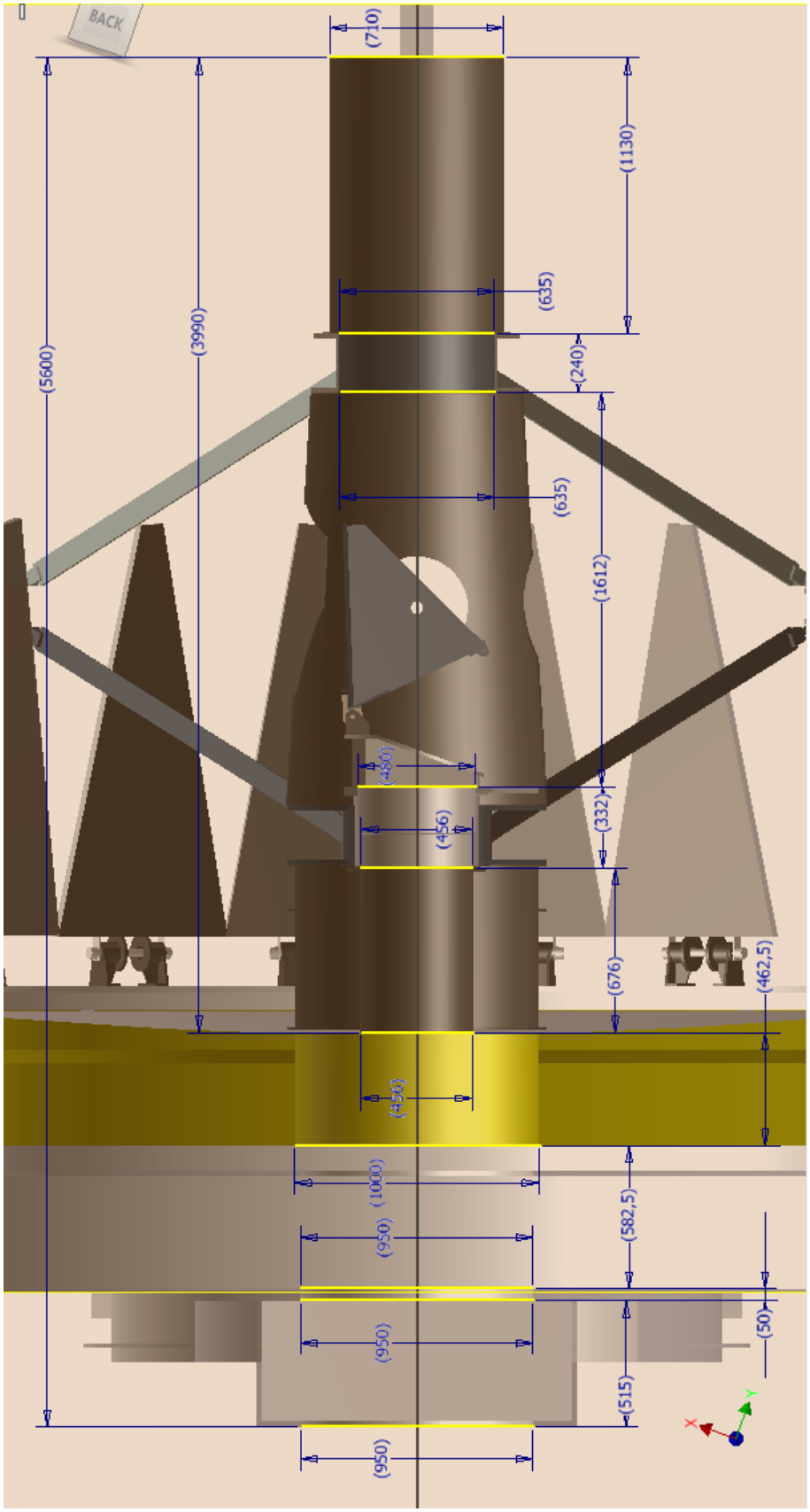
BACK
(710)
(1130)
(635)
(5600)
(3990)
(240)
(635)
(1612)
(480)
(456)
(332)
(676)
(462,5)
(456)
(1000)
(950)
(582,5)
(950)
(50)
(515)
(950)

C Scattered light with different baffles

Scattered light intensities are given for the d-nights of 9 and 10 August 2011. Different baffles have been tested on-sky and off-sky with a lamp. The numbers given are the angle from the moon/lamp in degrees, the peak intensity, and the background in counts.

9 August: off-sky tests with a 100 V lamp source. Exposure times are 0.5 seconds, and the ccd is 4x4 binned. At some large angles no exposures were taken to save time.

Without baffle			with ACAM baffle		
angle	peak	background	angle	peak	background
4	1400	1400	4		
6	4200	1900	6	8000	2500
8	34000	5000	8	28000	4000
10	38000	8000	10	38000	8000
12	28000	8000	12	28000	8000
14	22000	6000	14	22000	6000
16	5000	1600	16	5000	1600
18	1100	1100	18	1100	1100
20	1100	1100	20	1100	1100
22	1100	1100	22	1100	1100
24	1400	1400	24	1400	1400
26	3300	2200	26	3300	2200
28	2600	2100	28	2600	2100
30	2100	1800	30	2100	1800
32			32	1500	1300
35	1500	1300	35		
40	1200	1150	40		
45	1100	1100	45		
50	1100	1100	50		

10 August: On-sky tests with the moon. Baffles were placed in the areas mentioned in row 1.

ACAM, turret, sky fog baffle and L1			ACAM, turret and L1			Sky fog baffle and L1		
angle	peak	background	angle	peak	background	angle	peak	background
4	55000	55000	4	32000	32000	4	32000	32000
6	30000	30000	6	20000	20000	6	18000	18000
8	19000	19000	8	13500	13500	8	15000	12000
10	12500	12500	10	10000	10000	10	12000	9000
12	10000	10000	12	7000	7000	12	8500	7000
14	7000	7000						
16	5500	5500	16	4400	4400	16	4800	4600
20	4000	4000	20	3500	3500	20	3400	3400
30	2300	2300	30	2200	2200	30	2000	2000
40	1700	1700	40	1700	1700			
50						50	1400	1400

10 August: On-sky tests with the moon. Baffles were placed in the areas mentioned in row 1.

ACAM and L1			L1		
angle	peak	background	angle	peak	background
10	8500	4000	10	15000	10000
8	5500	4500	8	15000	14000
12	7000	4000	12	11000	8000
20	4400	4000	20	4000	3600